TWIST1 expression is associated with high-risk Neuroblastoma and promotes Primary and Metastatic Tumor Growth

Maria-Vittoria Sepporta[1], Viviane Praz[1,2], Katia Balmas Bourloud[1], Jean-Marc Joseph[3], Nicolas Jauquier[3], Nicolo' Riggi[2], Katya Nardou-Auderset[1,4], Audrey Petit[5,6], Jean-Yves Scoazec[7], Hervé Sartelet[5,8], Raffaele Renella[1], Annick Mühlethaler-Mottet[1*]

[1]Pediatric Hematology-Oncology Research Laboratory, Woman-Mother-Child Department, Lausanne University Hospital and University of Lausanne, Switzerland;

[2]Experimental Pathology, Lausanne University Hospital and University of Lausanne, Switzerland;

[3]Pediatric Surgery, Woman-Mother-Child Department, Lausanne University Hospital and University of Lausanne, Switzerland.

[4]Ophthalmic Hospital Jules-Gonin - Fondation Asile Des Aveugles, Lausanne, Switzerland

[5]Department of Pathology, Medical University of Grenoble, Grenoble, France

[6]Pediatric Hematology Oncology Department, CHU de la Timone, Marseille, France

[7]Department of Biology and Medical Pathology, Gustave Roussy Institute, Villejuif, France

[8]Department of Biopathology, CHRU de Nancy, Université de Lorraine, Nancy, France

*Contact information: Annick.Muhlethaler@chuv.ch

Keywords: Neuroblastoma, TWIST1/2, Metastasis, Extracellular Matrix, Myofibroblasts, Tumor Microenvironment, Tumor-Stroma Crosstalk

Abstract

The embryonic transcription factors TWIST1/2 are frequently overexpressed in cancer, acting as multifunctional oncogenes. Here we investigate their role in neuroblastoma (NB), a heterogeneous childhood malignancy ranging from spontaneous regression to dismal outcomes despite multimodal therapy. We first reveal the association of TWIST1 expression with poor survival and metastasis in primary NB, while TWIST2 correlates with good prognosis. Secondly, suppression of TWIST1 by CRISPR/Cas9 results in a reduction of tumor growth and metastasis in immunocompromised mice. Moreover, TWIST1 knockout tumors display a less aggressive cellular morphology and a reduced disruption of the extracellular matrix (ECM) reticulin network. Additionally, we identify a TWIST1-mediated transcriptional program associated with dismal outcome in NB and involved in the control of pathways mainly linked to the signaling, migration, adhesion, the organization of the ECM, and the tumor cells versus tumor stroma crosstalk. Taken together, our findings suggest TWIST1 as novel therapeutic target in NB.

Introduction

Neuroblastoma (NB) is the most prevalent solid extra cranial tumor of childhood[1]. While it accounts for approximately 5% of all pediatric cancer, it contributes for 12% of all pediatric deaths[2,3]. Primary tumors can arise along the sympathetic chains and in the adrenal medulla[1,4]. NB is both biologically and clinically heterogeneous. It spans from tumors with favorable biology that can spontaneously regress, to high-risk disease frequently relapsing or refractory to multimodal treatments and responsible for 50-60% of mortality[1,4]. Prognosis is associated with a number of factors, including International Neuroblastoma Risk Group (INRG) stages, age at diagnosis, histopathological classification, the presence of segmental chromosomal alterations[1,5], the activation of telomere maintenance mechanisms[6,7] and somatic mutations in the RAS/MAPK and p53 pathway[7]. Amplification of the proto-oncogene MYCN (MNA) is present in more than 20% of primary NB and in 40-50% of patients with high-risk (HR) disease. It is the most important biological predictor of a poor clinical response[2].

As for most pediatric cancers, the origins of NB can be linked back to defects in key cell signaling pathways during embryonic development[8]. NB originates from trunk neural crest (NC) progenitors that are committed to give rise to the sympathetic nervous system[4,8]. NC cells are a transient population of multipotent cells that, in the developing embryo upon an epithelial to mesenchymal transition (EMT), delaminate, migrate and differentiate into a broad lineage repertoire[9].

TWIST1/2 transcription factors are among the master regulators of the EMT process[10,11]. TWIST1/2 are highly conserved and guide developmental programs including cell lineage determination and differentiation, and are essential for organogenesis[10,12]. In humans, germline mutations of the TWIST1 gene are responsible for the Saethre-Chotzen syndrome (SCS), characterized by limb abnormalities, facial dimorphism, and premature fusion of cranial sutures[13]. Reactivation and aberrant functions of TWIST1/2 have been found in several carcinomas. Both TFs provide cells with critical properties including self-renewal capabilities, resistance to oncogene-induced failsafe programs and invasive capabilities thus promoting cancer initiation and progression toward a metastatic disease[10,11,14]. Since TWIST1/2 are active in NC cells, where they play a key role in driving EMT and migration, the study of their functions in NB is particularly important to better understand the neuroblastomagenesis, as distant metastases are already present by the time of diagnosis for the disseminated forms of this disease. So far, the role of TWIST1/2 in NB is still largely unknown. Upregulation of TWIST1 is found in NB with MNA and in a subset of no-MNA tumors, overexpressing MYCN or MYC[15-17]. In addition, TWIST1 protects NB cells from the pro-apoptotic effects mediated by MYCN, through the inhibition of the ARF/p53 pathway and cooperates with MYCN in NB to uphold both *in vitro* cell proliferation and *in vivo* tumor growth[15,18]. Recently, TWIST1 was also identified as a key regulator of MYCN-driven gene regulation through their cooperative binding on enhancers[18].

In this study, we initially revealed the correlation between the expression of TWIST1 and NB clinical prognostic factors *in silico* on primary NB gene expression datasets and in tumor tissue microarrays. Using an *in vivo* model for transcriptomic analyses, we then unveiled the impact of CRISPR/Cas9-mediated TWIST1 silencing on NB tumor growth, metastatic dissemination and the reorganization of the tumor microenvironment (TME).

Results

High levels of TWIST1 RNA expression are associated with poor outcomes in patients with NB.

In silico analysis using the CCLE database (https://portals.broadinstitute.org/ccle) shows that NB displays the highest levels of TWIST1 expression among 40 cancer cell lines, whereas TWIST2 is barely detected (Supplementary Fig. 1a). To further evaluate whether the expression levels of TWIST1/2 correlate with patient outcomes and NB prognostic factors, we analyzed two large clinical cohorts of primary NB tumors using the R2: Genomics Analysis and Visualization Platform (http://r2.amc.nl) (SEQC[19], n = 498; Kocak[20], n = 649). In both datasets, a high level of TWIST1 transcript strongly correlates with both a reduced overall survival (OS) (Fig. 1a; Supplementary Fig. 1b) and event-free survival (EFS) (Supplementary Fig. 1c).

97 Moreover, the expression of TWIST1 was more elevated in MNA NBs compared to those
98 without MNA (Fig. 1b, Supplementary Fig. 1d); and in higher stage tumors (stages 3 and 4 vs
99 1 and 2; stage 4 vs 4s) (Supplementary Fig. 1e).

100 To understand whether TWIST1 could be a prognostic factor in NB, we stratified patients of
101 the SEQC dataset according to the level of TWIST1 expression and either the MYCN status
102 (Fig. 1c) or risk (HR vs low-risk (LR); Supplementary Fig. 1f). For MNA or HR patients, TWIST1
103 expression level had no impact on the EFS. Conversely, for no-MNA and LR cases, a high
104 level of TWIST1 expression was associated with a reduced outcome, likewise the MNA or the
105 HR status, hinting to a possible role for TWIST1 as a prognostic factor for these patients. As
106 opposed to TWIST1, in the two same datasets, higher levels of TWIST2 were associated with
107 both a better OS and EFS in NB patients (Supplementary Fig. 1g). Moreover, TWIST2
108 expression was increased in no-MNA NB (Supplementary Fig. 1h).

109 **TWIST1 expression patterns reveal a correlation with poor prognostic factors in NB.**
110 We examined the expression levels of TWIST1/2 proteins in a NB tissue microarray (TMA)
111 (Table 1). In control sympathetic ganglia (SG), TWIST1 was not detected while TWIST2 was
112 present with moderate intensity in 46% of SG (Fig. 2a; Table 1). TWIST1 expression was
113 statistically significantly higher in tumors associated with poor prognosis: stages 3-4 vs stages
114 1-2; stage 4 vs 4s; tumors with MNA vs no-MNA; and in patients older than 18 months at the
115 diagnosis (Fig. 2b; Table 1). On the other hand, the expression of TWIST2 was higher in
116 tumors with better prognosis: stages 1-2 vs stages 3-4 and in patients with no-MNA vs MNA
117 (Fig. 2b; Table 1). However, no statistically significantly differences in TWIST2 expression
118 were observed in stage 4s vs stage 4 or in relation with age at diagnosis (Fig. 2b). Finally,
119 TWIST1 was frequently expressed in metastases (76% positive, median score=0.95), while
120 TWIST2 expression was uncommon (30% positive, median score=0.31) (Fig. 2a; Table 1).

121 **TWIST1 KO impairs the neurosphere-forming ability of NB cells.**
122 To investigate the contribution of TWIST1 in the aggressive features of NB, three cell lines,
123 either MNA (LAN-1 and SK-N-Be2c) or non-NMA (NB-1), were chosen for a TWIST1 knockout
124 (KO) through CRISPR/Cas9. A complete KO of the wild type (wt) TWIST1 protein expression
125 was obtained with the sgTWIST1 #1 for the three cell lines that from now on will be referred to
126 as sgTWIST1 cells (Supplementary Fig. 2a, b). TWIST1 KO did not significantly affected the
127 2D growth property of NB cell lines (Supplementary Fig. 2c), however it reduced the
128 neurosphere-forming ability of the three NB cell lines (Fig. 3a). Consequently, the number of
129 sgTWIST1 cells recovered from primary neurospheres was statistically significantly lower
130 compared to Control cells (Fig. 3a), indicating the role played by TWIST1 in propagating a
131 highly tumorigenic subpopulation of NB cells.

132 **TWIST1 KO delays tumor growth of NB xenotransplantation and extends survival in**
133 **mice.**
134 Next, we investigated the contribution of TWIST1 in the tumorigenicity of NB cells. In three
135 independent experiments, athymic Swiss nude mice were injected with the SK-N-Be2C Control
136 and sgTWIST1 cells either orthotopically (500'000 cells for ortho_1 and 50'000 cells for
137 ortho_2) or subcutaneously *(sc,* 250'000 cells). In all the three models, the growth of the
138 sgTWIST1 tumors was severely delayed compared to Controls thus extending sgTWIST1 mice
139 survival (Fig.3b, Supplementary Fig. 3a). In particular, in the first orthotopic experiment
140 (ortho_1), 26 days after the injection, tumors in Control mice were already above the pre-
141 determined volume for sacrifice while in the sgTWIST1 mice they were still in the lag phase
142 (Fig. 3c). In the second orthotopic experiment (ortho_2), we observed a significant delay in the
143 time of both SK-N-Be2c-sgTWIST1 tumor initiation and tumor growth (Fig.3d). Furthermore,
144 25 days after sc injections, the size of Control tumors was ~10 times larger than sgTWIST1
145 tumors. The latter required four additional weeks before reaching the size limit for sacrifice
146 (Supplementary Fig.3b). Finally, in both orthotopic experiments we observed SK-N-Be2c-
147 Control tumors invading the vena cava (n=3/6: ortho_1; n=3/8: ortho_2) (Supplementary Fig.
148 3c), whereas no invasion was detected in the sgTWIST1 mice group.

149 **TWIST1 KO diminishes the malignant phenotype of tumors and decreases**
150 **intrapulmonary macrometastasis**
151 In both orthotopic *in vivo* models, Control tumors presented histological features corresponding
152 to undifferentiated or poorly differentiated cells, while sgTWIST1 tumors were more
153 differentiated (Fig.4a). Moreover, Control cells showed a lower degree of cohesion and a
154 higher degree of immune cell infiltration compared to the sgTWIST1 tumors (Fig. 4a). We
155 analyzed the effects of TWIST1 KO on the pattern of collagen III/reticulin fibers, which
156 contribute to the ECM. Throughout all the three *in vivo* models, in Control tumor tissues the
157 continuity of the reticular fiber framework was lost in extensive tumor areas, and we observed
158 irregular thickening and fraying of fibers mainly at the borders of tumors (Fig. 4b,
159 Supplementary Fig. 4a). In contrast, the sgTWIST1 tumors were characterized by a preserved
160 reticulin mesh, resembling that of the normal adrenal gland (AG) (Fig. 4b, Supplementary Fig.
161 4a). This effect was not altered by the tumor size at the sacrifice (Supplementary Fig. 4b).

162 We speculated that the abovementioned ECM modifications associated with the expression of
163 TWIST1 could be responsible for a "pro-neoplastic" stromal phenotype, offering less resistance
164 for the invasive cells to escape the primary tumor site and form metastasis[21]. Therefore, the
165 lungs of the ortho_2 experiment mice were stained by H&E and anti-mCherry for the presence
166 of intrapulmonary metastasis (Fig. 4c). We could observe a decrease in the number of
167 intrapulmonary micrometastases (area (A) <1000 μm2) in the sgTWIST1 group, though this

168 difference was not statistically significant (Fig. 4d). Conversely, the number of intrapulmonary
169 macrometastases (A> 1000 µm2) in the sgTWIST1 mice was statistically significantly reduced
170 (Fig. 4d) as a single one was detected in only 1/10 sgTWIST1 mouse ($2.3x10^3$ μm^2) (Fig. 4c,
171 lower panel), whereas 6/8 Control mice had multiple macrometastases (mean
172 macrometastases size/mice: $5.1x10^5 \mu m2$).

173 **Identification of distinct transcriptional program regulated by TWIST1 and MYCN in NB**
174 **cells**

175 Transcriptomic analyses of SK-N-Be2c-Control and –sgTWIST1 cells and their derived-
176 ortho_1 tumors were performed by RNAseq. Principal Component Analysis (PCA) revealed a
177 high degree of segregation of the transcriptomic profiles of Control and sgTWIST1 for both
178 cells and ortho_1 tumors, enabling the accurate identification of genes that are differentially
179 expressed (DE) (Fig. 5a). We identified 2342 DE genes (1401 up- and 941 down regulated) in
180 SK-N-Be2c cells (Supplementary Fig. 5a; Supplementary Data 1) and 2013 (1003 up- and
181 1010 down regulated) in the SK-N-Be2c ortho_1 tumors (Fig. 5b; Supplementary Data 1), with
182 1213 found in common (Supplementary Data 1). Gene ontology (GO) analyses for the DE
183 genes in cells and in tumors reported a number of significantly enriched terms related to
184 signaling, nervous system development, migration, proliferation, ECM organization and
185 adhesion for both biological processes (BP) and cellular components (CC) (Fig. 5c;
186 Supplementary Fig. 5b; Supplementary Data 2).

187 As downregulation of MYCN was observed upon transient TWIST1 silencing in SK-N-Be2c, a
188 decrease in MYCN expression level could be, in part, responsible for the deregulation of the
189 transcriptional program observed in our ortho tumors[18]. To exclude this possibility, we analyzed
190 the expression level of MYCN protein by immunoblotting in tumors coming from the three in
191 vivo experiments. In all sgTWIST1 tissues, we detected an increase in the level of MYCN
192 protein compared to the Control counterpart (Supplementary Fig. 5c) although this increase
193 was not sufficient alone to promote and sustain a more aggressive phenotype in the sgTWIST1
194 tumors.

195 To compare the transcriptional program defined by TWIST1 with the one induced by MYCN in
196 SK-N-Be2c cells, we reanalyzed RNAseq data obtained upon MYCN shutdown using the BET-
197 bromodomain inhibitor JC1[18]. GO analyses performed on DE genes highlighted an enrichment
198 of gene sets mainly involved in the regulation of cell cycle and the DNA replication for both BP
199 and CC, thus suggesting distinct functions for the two TFs (Fig. 5d; Supplementary Fig. 5d;
200 Supplementary Data 3 and 4).

201

202

203 **A TWIST1-mediated gene expression signature is associated with poor outcome in NB**
204 We combined our ortho_1 transcriptomic analysis with RNAseq data of primary NB tumors to
205 identify a TWIST1-associated gene signature relevant in primary NB. Using the 'R2 Platform,
206 we first listed the genes either correlated (R positive) or anti-correlated (R negative) with
207 TWIST1 expression in the SEQC dataset of NB tumors (n=7737 genes with R absolute value
208 >0.225, Supplementary Fig. 6a). Second, we crossed this list of genes with the 2011 DE genes
209 between SK-N-Be2c-Control and -sgTWIST1 tumors, either up- (FC positive) or down-
210 regulated (FC negative) by TWIST1. We found 763 genes in common (Fig. 6a; Supplementary
211 Data 5) among which we selected those that had both R and FC either positive (172 genes) or
212 negative (317 genes). We called these resulting 489 genes the TWIST1-signature (Fig. 6b;
213 Supplementary Data 5). Using the same SEQC dataset, we analyzed the clinical significance
214 of the signature, and observed that genes correlated with TWIST1 in NB patients and
215 upregulated by TWIST1 in ortho_1 tumors (R and FC positive) mostly had an elevated level of
216 expression in high-risk, more advanced stages and MNA tumors. In addition, these tumors
217 displayed a low level of expression of genes downregulated in the TWIST1-signature (Fig. 6c).
218 Finally, an elevated expression level of the TWIST1-signature was associated in the SEQC
219 and Kocak datasets with a poor OS and EFS for both the complete patient cohorts and the
220 sub-cohorts without MNA (Fig. 6d, 6e; Supplementary Fig. 6 b, 6c).

221 Among the top deregulated genes in the TWIST1-signature, several have crucial roles during
222 embryonic development, in particular for the correct development of the nervous system
223 (*BMP7*, *FGF2*, *DTNA*, *MATN2*, *PCDHA1*, *PMP22*, *SCL1A3*). Moreover, most of the top up-
224 regulated genes are involved in the organization of both TME (*PDGFRA*, *VCAN*, *BMP7*, *FGF2*)
225 and ECM (*ADAMST19*, *PCOLCE*); in the EMT process (*BMP7*, *TRIM28*), as well as in cell
226 proliferation (*FGF2* and *PDGFRA*) and apoptosis (*BMP7*) (Fig. 7a). Besides, among the top
227 genes down-regulated in the TWIST1 signature, some are involved in neuronal differentiation
228 (*PIRT*), and various are tumor suppressor genes (*SYT13*, *FAM134B*, *PMP22*, *C7* and *MATN2*)
229 Fig. 7a). Several transcripts belonging to the TWIST1-signature were chosen, based on their
230 degree of differential expression and their biological function, for validation by RT-qPCR and
231 WB/IHC. We confirmed that *VCAN*, *PDGFRA*, *TRIM28*, *PCOLCE* and *ADAMTS19* genes were
232 upregulated by TWIST1, as their RNA and/or protein expression levels were increased in SK-
233 N-Be2c-Control relative to -sgTWIST1 tumors, while the opposite was true for the genes
234 downregulated by TWIST1 (*PIRT* and *SYT13*) (Fig. 7b-d; Supplementary Fig. 7a, 7b;
235 Supplementary Fig. 8a-c).

236 **TWIST1 alters the level of expression of genes involved in tumor-stroma crosstalk.**
237 Cancer cells establish a reciprocal intercellular signaling network and communicate with
238 stromal and immune cells via the production of soluble paracrine factors and their cognate

239 receptors. This complex signaling network shapes the TME to sustain cancer cell proliferation
240 and invasion. To address whether TWIST1 alters the expression of factors involved in cell-cell
241 communication, DE genes annotated as cytokines, chemokines, growth factors, inflammatory
242 mediators and their receptors, as well as integrin and their ligands were extracted from SK-N-
243 Be2c tumor transcriptome. This TWIST1-tumor-stroma signature is composed by 77 DE
244 genes, 33 up- and 44 down-regulated (Fig. 8a, Supplementary Data 6). Several play a pivotal
245 role in the regulation of focal adhesion (*EGFR*, *ITGA11*, *ITGA6*, *PDGFRB*); cell migration
246 (*COL5A1*, *ITGAV*, *ITGB3*, *PDGFRB*, *TGFB1*); proliferation (*FGF1*, *FIGF*, *IFI16*); angiogenesis
247 (*ACKR3*, *ACVRL1*, *EGFL7*, *FGF1*, *FGFR2*, *FIGF*); and inflammatory and immune responses
248 (*NGFR*, *TNF*, *TNFRSF1A*, *TNFRSF1B*, *TNFRSF4*, *TNFRSF9*, *TNFSF12*, *TNFSF13*,
249 *TNFSF4*). A high level of expression of the TWIST1-tumor-stroma signature was associated
250 with a poor OS and EFS of NB patients both in the SEQC (Fig. 8b) and the Kocak dataset
251 (Supplementary Fig. 9a).

252 To validate the tumor-stroma signature at the protein level and further characterize TWIST1-
253 mediated alterations in cell-cell communication, we analyzed the secretome of SK-N-Be2c-
254 Control and -sgTWIST1 cells *in vitro* by HPLC/Tandem MS using their conditioned media (CM)
255 containing both secreted proteins and extracellular vesicles released by tumor cells. These
256 secretomes contained 673 DE peptides (304 up- and 369 down-regulated) (Fig. 8c;
257 Supplementary Data 7) that corresponded to 678 genes. GO analyses revealed an enrichment
258 of BP linked to nervous system development, signaling, response to stimuli, migration, and
259 proliferation (Supplementary Fig. 9b; Supplementary Data 8).

260 Crossing secretome and transcriptome data from both cells and tumors, we identified 131
261 commonly deregulated terms, whereas 75 and 55 were uniquely shared between the
262 secretome and either the cell or tumor transcriptome, respectively (Fig. 8d; Supplementary
263 Data 7). Finally, after crossing the TWIST1-tumor-stroma signature with the secretome of cells,
264 we could identify 17 commonly DE terms, among which 14 were also found to be in common
265 with the transcriptome of cells (Fig. 8e). Most of the commonly deregulated terms were up
266 regulated by TWIST1 and annotated as growth factors, and for all terms but *COL5A1* and *VGF*,
267 the impact of TWIST1 on RNA and protein expression was always found to be correlated.

268 **Myofibroblast-associated gene expression is reduced in the stroma of sgTWIST1**
269 **orthotopic tumors.**

270 Among the terms deregulated in the abovementioned tumor-stroma signature, several are also
271 known for being involved in the crosstalk between cancer cells and the resident and recruited
272 stromal cells (i.e. *TGFB1*, *HGF*, *FGF*, *FGFR*, *EGFR*, *PDGFR*, *CXCL12*) and thus they could
273 mediate a TME sustaining the tumor growth[22]. One of the main stromal changes within a pro-

274 tumorigenic TME is the appearance of cancer-associated fibroblasts (CAFs), playing a critical
275 role in arranging the "soil" within which tumor cells proliferate[23]. To verify whether we could
276 detect the presence of CAFs in the tumor stroma, the ortho_1 RNAseq data were aligned with
277 the murine genome. Between Control and sgTWIST1 tumors, 89 stromal genes were found to
278 be DE(69 up- and 20 down-regulated) (Fig. 9a; Supplementary Data 9). Genes up-regulated
279 in the stroma of TWIST1 expressing Control tumors showed a significant enrichment of muscle
280 contraction-related terms (Fig. 9a; Table 2). This was defined as the myofibroblastic signature
281 (n=36 genes) according to the literature[24-27]. GO analysis for the murine DE genes reported a
282 number of statistically significantly enriched terms related to sarcomere organization and
283 muscle contraction (Fig. 9b, Supplementary Data 10), supporting a TWIST1-mediated
284 recruitment and activation of myofibroblasts.

285 Besides, among the up-regulated genes, we noticed the Macrophage Receptor with
286 Collagenous Structure (Marco), which defines a subtype of alternatively-activated M2 tumor-
287 associated macrophages (TAMs) with immunosuppressive functions and involved in tumor
288 progression[28]. Six up-regulated genes of the myofibroblastic signature (*Pvalb*, *Neb*, *Acta1*, *Ttn*,
289 *Myh1*, *Msln*) (Supplementary Fig. 10a) and *Marco* were confirmed by RT-qPCR. For the
290 selected genes of the signature, a reduction in their RNA expression levels was observed in
291 both ortho_sgTWIST1 tumor stroma only, and were undetectable in the tissues from the sc
292 tumors (Fig. 9c, Supplementary Fig. 10b). The reduced RNA expression level of *Marco* in
293 sgTWIST1 tumor stroma was validated in all the three *in vivo* models (Fig. 9c, Supplementary
294 Fig. 10b). Finally, qualitative validation by IHC with the CAF marker fibroblast-activation protein
295 (Fap) confirmed the presence of CAFs in both Control and sgTWIST1 ortho_1 tumors (Fig.
296 9d).

297 To analyze the potential interactions existing between the TWIST1-associated tumor-stroma
298 signature and the DE stromal genes, a protein-protein interacting (PPI) network was
299 constructed using the STRING website (https://string-db.org/).The two groups of DE genes
300 clustered separately and had a high level of linkage both among genes of each category and
301 reciprocally (Fig. 10). Two stromal genes reported as myofibroblastic markers, *Acta1*,
302 belonging to the actin family and *Actn2*, a member of the spectrin superfamily, were strongly
303 linked to the network of myofibroblastic genes and connected with the tumor gene cluster, via
304 *TGFB1*, *TGFB3*, *HGF*, *LAMC3* and *LAMA5*, *FIGF* and *HSPB1*[29,30].

305

306

307

308 ## Discussion

309 In this study, we discovered a role for the embryonic TFs TWIST1 and TWIST2 as prognostic
310 factors in NB. We could reveal the contribution of TWIST1 in enhancing primary and secondary
311 tumor growth and in mediating an aggressive phenotype in *in vivo* NB xenografts. Furthermore,
312 we identified a TWIST1-associated transcriptional signature, which correlated with outcomes
313 in human primary tumors and activated the TME in an orthotopically-derived xenograft murine
314 model.

315 TWIST1 and TWIST2 have previously been described as playing a distinct role during
316 embryonic development and having anti-correlated transcriptional expression patterns in
317 spontaneous focal mammary tumors in mice and in human melanoma, colon, kidney, lung and
318 breast cancer[31]. In this study, we show their opposite expression pattern in primary NB and
319 their antithetical prognostic value, highlighting that theTWIST1 expression was correlated with
320 unfavorable NB prognostic factors, metastasis and poor survival. These findings are in line
321 with prior studies conducted on non-pediatric cancers showing the overexpression of TWIST1
322 in high grade and invasive/aggressive breast, bladder, cervical, ovarian and hepatocellular
323 cancers where it might also serve as prognostic factor for poor survival[32]. Moreover, we
324 confirmed previous data showing the association of TWIST1 with MNA NB on larger cohorts
325 of patients[15,16]. Furthermore, TWIST2 was mainly detected in normal tissues and in NB with
326 better prognosis. These results are in contrast with those obtained by others, showing an
327 association between the upregulation of TWIST2 and a more aggressive tumor phenotype[33-
328 36]. Importantly, we identified TWIST1 as a valid candidate in predicting the poor outcome of
329 patients with no-MNA or LR NB, in the same way as the amplification of MYCN or the HR
330 classification.

331 Our *in vivo* investigations on the biological effects of TWIST1 reveal that its loss delays the
332 primary tumor initiation and growth of NB, regardless of the number of cells and the injection
333 site. These data are aligned with prior evidence showing that the suppression of TWIST1
334 hampers the growth of primary skin papilloma induced by carcinogens[37]; and that the
335 pharmacological inhibition of the Twist-BRD4-Wnt5a signaling axis results in the reduction of
336 tumorigenicity of basal-like breast cancer[38]. Moreover, the overexpression of TWIST1
337 accelerates tumor establishment and growth of MCF-7-derived breast cancer and transforms
338 mouse embryonic fibroblasts in cells with high tumorigenic potential[31,39]. In contrast with these
339 findings, TWIST1 was shown as nonessential for primary tumor initiation and growth in several
340 *in vivo* murine models for breast cancer, pancreatic ductal adenocarcinoma and hepatocellular
341 carcinoma, although it seems to play a pivotal role in driving cells migration and invasion[14,40,41].
342 Taken together, these antithetical findings suggest that the role of TWIST1 in carcinogenesis
343 might depend upon the tumor settings as well as on oncogenic drivers.

344 In our experiments, TWIST1-expressing tumors displayed a phenotype typical of less
345 differentiated NBs. Additionally these tumors were characterized by abundant fascicules of
346 spindle-shaped cells, typical of a mesenchymal-like morphology. The role played by TWIST1
347 in driving the EMT and in maintaining cells in a mesenchymal state has been widely
348 documented as part of both the morphogenesis during embryonic development, and in the
349 pathogenesis of multiple types of invasive cancers[41-44]. Moreover, several studies demonstrate
350 an association between the EMT and the acquisition of stem-like characteristics in normal and
351 neoplastic epithelial tissues, identifying in TWIST1 the molecular linker between these two
352 biological processes[45-47]. In our study, TWIST1-expressing NB cells were able to grow *in vitro*
353 as neurospheres, known to be enriched in tumor-initiating cells (TIC) exhibiting stem-like
354 features[48]. Furthermore, our data reveals a role for TWIST1 in metastatic dissemination in NB,
355 as an increase in the number and in the size of pulmonary metastases was observed in Control
356 mice. In fact, the decrease of the invasive mesenchymal-type cells in the sgTWIST1 tumors
357 and the reduced ability of sgTWIST1 cells to maintain the TIC population could at least in parts
358 explain the reduction in the number of pulmonary micrometastases observed in sgTWIST1
359 mice. Moreover, the suppression of TWIST1 also had an impact on the last step of the
360 metastatic cascade, the colonization, consisting in the growth of micrometastases into
361 macroscopic metastases, that lies on the self-renewal capability and the proliferative potential
362 of invading cells.

363 The ECM is another key player in promoting tumor invasion and metastasis. Disruption and
364 stiffness of this framework has been demonstrated to contribute to malignant transformation
365 and cancer progression by destabilizing the cell–cell adhesions and promoting cell
366 invasion[21,49]. In Control tumors expressing TWIST1, we observed a disruption of the reticulin
367 mesh, one of the main components of the ECM, and an increase in their density along the
368 tumor border. In contrast, sgTWIST1 tumors preserved a nest-like arrangement of thin reticular
369 fibers, as observed in the normal adrenal gland. Interestingly, a disorganized and cross-linked
370 reticulin network was associated with poor NB prognosis, and a morphometric classification
371 based on variations of both blood vessels and reticulin fibers shape and size was proposed to
372 identify ultra-high risk NB patients[50]. The involvement of TWIST1 transcriptional targets in the
373 degradation/remodeling of the ECM has been demonstrated in both normal embryonic
374 development as well in cancer[21,42,51-53]. In our orthotopic model, we found several genes
375 involved in the organization of the ECM and the TME, such as *VCAN*, *ADAMTS19*, *PDGFRA*,
376 *TRIM28* and *PCOLCE*, among the top 20 upregulated by TWIST1, suggesting a role for
377 TWIST1 in defining a permissive microenvironment contributing to the survival and
378 maintenance of cancer stem-like cells. *PCOLCE* is a direct transcriptional target of TWIST1
379 and is implicated in the regulation of collagen deposition during both early craniofacial

380 development and in osteosarcoma, where it promotes tumor growth, cell migration and
381 invasion[42,54] . In our study using two cohorts of primary NB, *PCOLCE* was the gene presenting
382 the highest correlation with TWIST1 expression regardless of the amplification status of
383 MYCN, suggesting a role for TWIST1 in the control of *PCOLCE* expression also in primary NB.

384 For the first time, we identified a NB-associated TWIST1-signature by combining the
385 transcriptomic data of orthotopic tumors with that of primary tumors. Importantly, an elevated
386 expression of this signature was found in MNA and HR tumors, and it was associated with poor
387 survival in the entire NB datasets and their sub-cohorts without MNA. In addition, a subgroup
388 of TWIST1-target genes involved in shaping the interface between tumor cells and its stroma
389 could be extracted, which we named TWIST1-tumor-stroma signature. Both signatures
390 induced by TWIST1 were linked to poor survival *in silico*, indicating their biological relevance
391 and confirming the functional role of TWIST1 in NB pathogenesis.

392 The cooperation between TWIST1 and MYCN in defining a transcriptional program in NB
393 supporting *in vitro* cell proliferation and *in vivo* tumor growth has already been shown[15,18]. Using
394 our results and previous published findings on NB, we conclude that these TFs seem to
395 orchestrate distinct functions. Indeed, GO analysis on our transcriptomic data revealed that
396 suppression of TWIST1 in SK-N-Be2c cells and tumors mainly deregulated pathways involved
397 in signaling, nervous system development, migration, adhesion, ECM organization, and cell
398 proliferation. Interestingly, these pathways were also principally deregulated by the genes
399 enriched in the TWIST1-signature. On the other side, GO analysis performed on RNAseq data
400 of SK-N-Be2c cells downregulated for MYCN through JC1[18] highlighted a major role for MYCN
401 in controlling the cell cycle regulation and DNA replication. Similar pathways were also
402 identified upon MYCN silencing through JC1 or shRNA in MNA NB cell lines [55], thus confirming
403 a predominant role for this TF in supervising mostly the proliferation of cells.

404 There are several limitations in our study. First, the use of only one NB cell line to obtain our
405 *in vivo* model could represent an issue in the wider relevance of our findings. Although SK-N-
406 Be2c cells are commonly used for NB research, they in fact might not fully represent the biology
407 and diversity of the disease itself. Thus, our observations about the role of TWIST1 in
408 enhancing NB tumor aggressiveness remain to be verified using NB cell lines without MNA as
409 well as primary NB cells. Second, RNAseq analysis was performed on tumors of the ortho_1
410 experiment, which did not give rise to macroscopic metastases. This was probably caused by
411 extremely rapid tumor growth, which might have prevented the formation of macrometastases.
412 However, this model is suitable for appreciating the effects of TWIST1 on tumor growth
413 capacity and phenotypic features as well as on TME remodeling. Moreover, the main
414 deregulated genes and pathways were consistently altered by TWIST1 between SK-N-Be2c

415 cells and ortho_1 tumors, and the most relevant genes were confirmed in the ortho_2 tumors.
416 Importantly, the biological relevance of the transcriptional program defined by TWIST1 in the
417 SK-N-Be2c ortho_1 xenografts were validated in human primary NB, with the identification of
418 a TWIST1-associated signature and a tumor-stroma signature, both displaying a strong
419 prognostic impact in two cohorts of NB patients. Third, in our study we only focused on the
420 incidence of metastases in the lungs of mice, which occurs in approximately 4% of children
421 with newly diagnosed NB[56]. We did not detect macrometastases in the liver, one of the most
422 frequent sites of infiltration in children together with bone marrow, bone, and lymph nodes.
423 Fourth, the unambiguous identification of the stromal counterpart activated by the tumor-
424 stroma signature remains challenging. Our transcriptomic data suggest an enrichment of M2
425 TAM and of myofibroblasts, the most abundant stromal cells supporting tumor progression, in
426 TWIST1-positive xenografts. The marked connection observed between the TWIST1-tumor-
427 stroma signature and the stromal DE genes by STRING analysis further support their role in
428 mediating the NB-associated alterations in the tumor stroma. However, the qPCR validation of
429 the stromal genes belonging to the myofibroblastic signature was hampered by sometimes
430 extremely low/undetectable expression levels. This was probably due to the very limited
431 number of stromal cells present in whole tumor lysates. Single cell sequencing could further
432 facilitate the characterization of the impact of TWIST1 on stroma composition. Moreover, it
433 could be argued that an immunocompromised mouse model does not represent the most
434 suitable setup to study TME components. Genetically engineered models spontaneously
435 developing tumors or humanized mouse NB models could represent other valid alternatives to
436 recapitulate the TME composition in NB[57]. Finally, precisely identifying CAF by IHC remains
437 difficult due to the lack of specific myofibroblast markers, a common issue in all studies.

438 In summary and for the first time, our study revealed the prognostic significance of TWIST1
439 and TWIST2 in NB. The biological impact of TWIST1 on tumor growth and metastatic formation
440 capacity was associated with alterations in the ECM composition and with the establishment
441 of a TME supportive of tumor growth and progression. The transcriptional program activated
442 by TWIST1 in our *in vivo* model of NB further supported these findings and its validation in
443 primary NB unveiled a correlation with HR disease and poor prognosis. All our findings strongly
444 indicate a very promising role for targeting TWIST1 in the therapy of HR or relapsed/refractory
445 NB, which remains an almost universally fatal disease.

446

447

448

449 # Methods

450 **Cancer Cell Line Encyclopaedia (CCLE) database analysis**

451 The CCLE database (https://portals.broadinstitute.org/ccle) was used to compare the mRNA
452 expression level of TWIST1 and TWIST2 in a range of 36 different cancer types (Affymetrix
453 arrays: Affimetrix Human Genome U133, Plus 2.0). Quality filtering and normalization were
454 performed using Robust Multi-array Average (RMA) and quantile normalization.

455 **Tumor Microarray (TMA) and Immunohistochemistry**

456 The TMA was composed by 72 primary tumors, 25 matched metastases and 44 matched
457 control normal tissues (13 sympathetic ganglia and 31 adrenal glands) (Table 1) obtained from
458 72 patients diagnosed with NB between July 1988 and November 2001 treated and followed
459 at the Bicêtre hospital (Le Kremlin-Bicêtre) and the Gustave Roussy Institute (Villejuif).
460 Immunohistochemical study on patient tissues was performed after patients' informed consent
461 and according to the ethical regulations of the institution. On average, 4 tissue cores with a 0.6
462 mm diameter were obtained and transferred into a recipient paraffin block using a tissue
463 arrayer (Alphelys: Beecher Instruments Micro-Array Technology, Plaisir, France). TMA
464 sections 5-µm were made on Benchmark XT Ventana (ROCHE Diagnostics). After dewaxing,
465 antigen retrieved is performed using water-bath heating in the following buffers: in citrate buffer
466 pH 6.0 (CC2 citrate-based buffer Ventana Medical Systems ROCHE Diagnostics) for TWIST1
467 and in a CC1 buffer of pH 8 (CC1 = Tris-Borate/ EDTA, Ventana Medical Systems ROCHE
468 Diagnostics) for TWIST2. Slides were then incubated 1h at RT with the rabbit polyclonal anti-
469 TWIST1 (1/50, ABD29, Millipore, Burlington; MA, USA); or 1h at 37°C with the sheep polyclonal
470 anti-TWIST2 (1/200, AF6249, R&D Systems, Minneapolis, MN, USA) in Antibody Diluent
471 Buffer from Ventana Medical Systems, ROCHE Diagnostics. The detection kit for the
472 antibodies is the UltraView DAB detection Kit (Ventana Medical Systems Inc./ Roche
473 Diagnostic). A counter-staining of the nuclei was used for 12 minutes by Hematoxylin.
474 Immunostaining scores (0–4) were established for each stained tissue by semi-quantitative
475 optical analysis by two independent investigators blinded for clinical data. The percentage of
476 positive cells in each sample was scored as follows: 0, all cells negative; 1+, up to 25% of cells
477 were positive; 2+, 26% to 50%; 3+, 51% to 75%; 4+, more than 75%.

478 **Cell culture**

479 The established human MNA NB cell lines (SK-N-Be2c and LAN-1) were obtained from their
480 lab of origine[58,59]. Authentication of SK-N-Be2c and LAN1 cell lines was performed by
481 microsatellite short tandem repeat analysis before starting the transduction experiments
482 (Microsynth, Switzerland). The no-MNA NB1-M primary cells were derived in our laboratory
483 from a bone marrow tissue recovered at the diagnosis from a patient with NB at the
484 Hematology Oncology Unit of the University Hospital of Lausanne, Switzerland[48]. All cell lines

485 were cultured in Dulbecco's modified Eagle's medium (D-MEM) (Gibco, Paisley,UK),
486 supplemented with 1% penicillin/streptomycin (Gibco) and 10% heat inactivated Fetal Calf
487 Serum (FCS) (Sigma-Aldrich, St. Louis, Missouri, USA) and under standard culture conditions
488 in humidified incubator at 37°C with 5% CO2.

489 **TWIST1 knock out through CRISPR/Cas9 technology**

490 Two sgRNAs targeting the first exon of the TWIST1 gene were chosen in the published sgRNA
491 library[60]. Oligos were designed as follow: sgTWIST1-1: forward 5'-
492 CACCGCGGGAGTCCGCAGTCTTACG-3'; reverse 5'-
493 AAACCGTAAGACTGCGGACTCCCGC-3'; sgTWIST1-2: forward 5'-
494 CACCGCTGTCGTCGGCCGGCGAGAC-3'; reverse 5'-
495 AAACGTCTCGCCGGCCGACGACAGC-3'. The lentiviral vector lentiCRISPR v2[61] was
496 obtained from Adgene (Cambridge, USA). LentiCRISPR v2-sgTWIST1 plasmids were
497 constructed according to the manufacturer's instructions (Adgene), and used to transduce
498 Control cells. Virus production and lentiviral infections were performed as previously
499 described[62]. Transduced SK-N-Be2c, LAN-1 and NB1-M cells were selected 24 h post-
500 infection with either 5 µg/ml for SK-N-Be2c or 1 µg/ml for LAN-1 and NB1-M cells of puromycin
501 (Gibco). Clones were isolated by limiting dilution cloning in a 96-wells plate from the Control
502 and sgTWIST1 #1 of LAN-1 and SK-N-Be2c cell lines. Only clones derived from a single colony
503 were selected and further screened by Immunoblotting. To avoid potential problems caused
504 by variability during single-cell clonal expansion, we pooled 5 and 7 clones for the Control and
505 sgTWIST1 SK-N-Be2c cells, respectively; for the LAN-1 cells, 6 clones were pooled for both
506 Control and sgTWIST1 cells. SK-N-Be2c-Control and sgTWIST1 pools of cells were further
507 transduced with a lentiviral vector expressing the mCherry gene (Ex-NEG-Lv244 from
508 GeneCopoeia™). These cells expressing the mCherry gene were used for the ortho_2 and the
509 sc xenograft experiments. In addition, genome editing in SK-N-Be2c sgTWIST1 cells was
510 verified by NGS sequencing. Briefly, PCR amplicons were designed across the TWIST1
511 genomic regions targeted by the sgRNAs to examine generation of indels. A first PCR of 20
512 cycles was performed using the primers Twist1-nest-F: 5'-
513 GCAAGAAGTCTGCGGGCTGTGG-3' and Twist1-nest-R: 5'-
514 GGATGATCTTCCGCAGCGCG-3', followed by purification with QIAquick PCR purification kit
515 (QIAGEN). Then we run a second PCR of 10 cycles with nested primers containing Illumina
516 overhang adapter sequences: Illumina-P5-Twist1-F: 5'-
517 TCGTCGGCAGCGTCAGATGTGTATAAGAGACAG AAGAAGTCTGCGGGCTGTGGCG-3';
518 Illumina P7-Twist1-R: 5'-
519 GTCTCGTGGGCTCGGAGATGTGTATAAGAGACAGCGCTCCCGCACGTTGGCCATG-3'.
520 Both PCR were performed using the 2xKAPA HiFi HotStart ReadyMix as follow: 95°C for 5

521 minutes, 10 cycles at 98°C for 20 s, 73°C for 30 s, 72°C for 30 s; then 72°C for 5 min. Finally,
522 a third PCR was performed to attach Illumina adaptors and barcodes to samples according to
523 manufacturer's instructions. Amplicons were purified by using AMPure XP (Beckman Coulter,
524 Indianapolis, USA), and sequenced with a MiSeq Micro 300 (Illumina Inc., San Diego, USA) at
525 the Lausanne Genomics Technologies Facility (GTF)
526 (https://wp.unil.ch/gtf). After high throughput sequencing reads, PCR amplicons were checked
527 for indels using CRISPResso (https://crispresso.pinellolab.partners.org). The results of the
528 sequencing of the bulk population of SK-N-Be2c-sgTWIST1 cells, the 7 derived clones, and
529 the 4 sgTWIST1 ortho_1 tumors are shown in Supplementary Data 11. Surprisingly, in all the
530 sgTWIST1 clones we detected the same three main indels. Note that three alleles found in the
531 SK-N-Be2c cells, indicating a triploidy of this genomic region as previously described[63].

532 **Neurosphere Assay**

533 NB cells ($2x10^4$ cells/ml) were cultured in Neural Crest Stem Cell culture medium (NCSC)
534 [DMEM/F12 (Gibco) supplemented with 1 % penicillin/streptomycin (Gibco), 2 % B27 (Gibco),
535 20 ng/ml human recombinant bFGF (Peprotech, Rocky Hill, USA), 1% N2 (Gibco), 2-
536 Mercaptoethanol 50µM (AppliChem, Darmstadt, Germany) 15% Chicken Embryo Extract, 20
537 ng/ml IGF-1 (Peprotech), Retinoic Acid 110 nM], using poly-Hema-coated six wells plates to
538 prevent cell adhesion. After 7 days in culture, pictures of sphere were taken using an Olympus
539 IX53 inverted microscope (Olympus, Shinjuku, Japan) and acquired with the Olympus
540 cellSense imaging software. Spheres were dissociated with StemPro Accutase Cell
541 Dissociation Reagent (Gibco, A11105-01) and the number of cells recovered after the
542 dissociation of spheres was determined using the trypan blue exclusion method.

543 **Proliferation assay**

544 Briefly, $1.2*10^4$ MNA (SK-N-Be2c and LAN-1) and $3*10^4$ no-MNA (NB1-M) cells were seeded
545 in quadruplicate in 96-wells plate in DMEM/FCS. Cell proliferation was assessed using the
546 CellTiter 96® Aqueous Non-radioactive Cell proliferation Assay (Promega, Madison, WI, USA)
547 according to the manufacturer's protocol.

548 ***In vivo* studies**

549 Animal experiments were carried out with athymic Swiss nude mice (Crl:NU(Ico)-Foxn1^{nu};
550 Charles River Laboratory, France) in accordance with established guidelines for animal care
551 of the Swiss Animal Protection Ordinance and the Animal Experimentation Ordinance of the
552 Swiss Federal Veterinary Office (FVO). Animal experimentation protocols were approved by
553 the Swiss FVO (authorization numbers: VD2995 and VD3372). All reasonable efforts were
554 made to reduce suffering, including anesthesia for painful procedures. For surgical procedures,
555 mice were anaesthetized using isoflurane (Baxter, Deerfield, IL, USA) and received

556 paracetamol as analgesia the day before the surgery. Orthotopic implantations were performed
557 as previously described[64] with slight modifications: $5x10^5$ (ortho_1, 6 mice/group) and $5x10^4$
558 (ortho_2, 12 mice/group) SK-N-Be2c cells were resuspended in 10 µl of PBS and injected in
559 the left adrenal gland after a small incision above the left kidney. Tumor growth was followed
560 by ultrasound every 7 to 14 days at the Cardiovascular Assessment Facility (University of
561 Lausanne). For subcutaneous implantation, groups of 5 mice were injected in the right flank
562 with $2.5x10^5$ cells suspended in 200 µl 1:1 mix of DMEM and BD Matrigel™ Basement
563 Membrane Matrix (BD Biosciences, Bedford, MA, USA). The grafted animals were then weekly
564 monitored with calipers for tumor growth assessment. The tumor volume was calculated using
565 the formula: volume = 4/3 × π × (depth × sagittal × transversal)/6 for ortho tumors; and volume
566 = (length x $width^2$)/2 for sc tumors. For both orthotopic and subcutaneous implantations, mice
567 with tumor volumes around ~1000 mm^3 were sacrificed using CO_2. Tumors and organs (lungs,
568 liver) were cut into pieces and snap frozen in liquid nitrogen or fixed in formol and embedded
569 in paraffin (lungs, liver, kidneys and spleen).

570 **RNA isolation**

571 Total RNA from cell lines and tumors was extracted using RNeasy kit (Qiagen, Hilden,
572 Germany). RNA concentration was quantified using a Nanodrop (Agilent Technologies,
573 Wilmington, DE, USA). For the RNA sequencing, RNA was quantified using Qubit Fluorometer
574 (Life Technologies, Carlsbad, CA, USA).

575 **RNAseq library preparation**

576 RNAseq was performed at the iGE3 Genomics platform (University of Geneva,
577 https://ige3.genomics.unige/ch) using standard techniques RNA integrity was verified using
578 the Agilent 2100 Bioanalyzer system (Agilent Technologies). The total RNA ribo-zero gold kit
579 from Illumina was used for the library preparation with 1 µg or 500 ng of total RNA as input for
580 cells (n=3 biological replicates/group) and tumors (n=4/group), respectively. Library molarity
581 and quality were assessed with the Qubit and Tapestation using a DNA High sensitivity chip
582 (Agilent Technologies). Libraries were pooled at 2 nM and loaded for clustering on 1.5 lanes
583 for cells and 1.5 lanes for tumors of a Single-read Illumina Flow cell. Reads of 100 bases were
584 generated using the TruSeq SBS chemistry on an Illumina HiSeq 4000 sequencer.

585 **Bioinformatics analysis of RNAseq data**

586 For all samples, fastq files with 100 nucleotides long single-end reads were mapped with STAR
587 version 2.5.2b on both the Human genome version Hg19 and the Mouse genome version
588 Mm10, simultaneously. The following options were changed from the default parameters: --
589 outSAMmultNmax 50; --outFilterMatchNminOverLread 0.4; --quantMode TranscriptomeSAM.
590 Transcriptome annotations in gtf format for both organisms were downloaded from the

591 gencode website (https://www.gencodegenes.org/). Reads mapped on either the Human or
592 the Mouse transcriptome were then parsed and split in one file per organism with an in-house
593 perl script. Reads with matches on both Human and Mouse were discarded from the Mouse
594 file. Per-gene counts and rpkm were then extracted independently for each organism using
595 rsem version 1.3.0. All RNAseq per-gene data quality checks and analysis were done in R.
596 Mouse and Human data were analyzed independently, but following the same protocol. Protein
597 coding genes with a log2(rpkm) value above 1 in at least one sample were kept (13742 genes
598 in SK-N-Be2c for Human data; 14538 for Mouse data). Principal Component Analysis were
599 done using the normalized log2 (rpkm) values. Clustering analysis were performed on the
600 normalized log2 (rpkm) values using euclidean distance measures and the ward.D2
601 agglomeration method. Differential analyses were performed using the raw counts in DESeq2
602 package version 1.26.0. For each comparison, the cutoffs for fold-change (in log2) and
603 adjusted *p* values to call differentially transcribed genes were set to 1 and 0.05 for Human,
604 respectively, and to 0.5 and 0.05 for Mouse, respectively. Heat maps for sample correlations
605 and for specific gene lists were generated using the heatmap.2 function from the gplots
606 package version 3.0.1.2 on the log2 of DESeq2 normalized counts. Functional gene ontology
607 analysis was performed by applying a hypergeometric test on selected genes lists against
608 gene sets from KEGG, GO (Molecular Function, Biological Process and Cellular Component),
609 REACTOME, and BIOCARTA pathways. The *p* value cutoff for terms selection was set to
610 0.001 for Human data and to 0.01 for Mouse data; only those terms with an adj *p* value below
611 0.01 and 0.1 were taken into consideration for the graphical representation, respectively. For
612 the GO analysis of the secretome, the lines containing multiple gene references were split
613 before to apply the hypergeometric test on the resulting list of genes (673 terms in the
614 secretome vs 678 terms in the transcriptome). For external RNAseq data analysis (Super
615 series number: GSE80154; SubSeries number: GSE80153), fastq files from GSM2572350 to
616 GSM2572355 corresponding to Be2C samples at 0 (DMSO: GSM2572350 to GSM2572352)
617 and JQ1 24h (GSM2572353 to GSM2572355) were downloaded. These samples were then
618 re-analyzed by applying the same protocol used for the local RNAseq data.

619 **Real-Time qPCR**

620 cDNA were prepared from 0.5 or 1 µg of RNA for the validation of human or murine genes,
621 respectively using PrimeScriptTM reagent kit according to the manufacturer's instruction
622 (TAKARA Bio Inc., St.Germain-en-Laye, France). The expression level of selected genes was
623 validated by semi-quantitative real-time PCR using primer pairs described in Supplementary
624 Data 12 and the QuantiFast SYBR® green kit (Qiagen, Hilden, Germany). Cycling conditions
625 were: 5 min at 95°C, 40 cycles of 10 sec at 95°C, 30 sec at 60°C, and 1 sec at 72°C with the
626 Rotor Gene 6000 real-time cycler (Corbett, Qiagen). Gene expression levels were determined

627 by normalization to either HPRT1 (human genes) or β-actin (murine genes) housekeeping
628 genes using the ΔCt method.

629 **Immunohistochemistry**

630 Histopathological analyses were performed on blocks embedded in paraffin at the Mouse
631 Pathology Facility of Lausanne University (Epalinges, Switzerland) and at the Histology Core
632 Facility of the EPFL (Lausanne, Switzerland). Thin tumor sections (3 µm thick) were de-waxed
633 and rehydrated and then stained with hematoxylin and eosin; Gomori's for reticulin or type III
634 collagen detection, or IHC was performed using primary antibodies (Supplementary Data13).
635 Staining were imaged using an Olympus BX43 light microscope and then acquired with the
636 Olympus cellSense imaging software or using the EVOS5000 imaging system (Life
637 Technologies); or whole slides were scanned using the NanoZoomer S60 Digital slide scanner
638 C13210 (Hamamatsu, Japan) at the 20x magnification with a resolution of 0.46 µm/pixel.
639 Visualization and analyses of the scans was performed using the QuPath imaging software
640 (https://qupath.github.io). For the quantification of VCAN and α-mCherry, the entire surface
641 either of the tumor or of three subsequent lung sections separated by a depth of 100 µm has
642 been taken into consideration, respectively. Quantification was perfomed with the QuPath
643 software according to the following pipeline: select a region of the tumor (magnification:
644 12.48X), analyze, cell analysis, positive cell detection. Options modified from the default
645 parameters: image type: Brightfield (other); detection image: optical density sum; intensity
646 threshold parameters: threshold 1+: 0.3.

647 **Immunoblotting**

648 NB cells and SK-N-Be2c-derived ortho tumors were lysed in NP40 buffer (50 mM Tris-HCl pH
649 8.0; 150 mM NaCl; 1% NP-40 and 1x protease inhibitor cocktail (Complete mini, EDTA-free,
650 Roche, Mannheim, Germany). Cell lysates were centrifuged at 15'000 rpm at 4°C for 10 min.
651 Supernatants were recovered and protein concentrations were measured using Bradford
652 method (Bio-Rad Laboratories, Hercules, CA, USA). Equal amount of total protein lysate (40
653 µg for DE genes validation; 50 µg for TWIST1 and MYCN validation) was loaded onto 4-15%
654 precast polyacrylamide Mini-PROTEAN TGX gel (Bio-Rad Laboratories). Proteins were
655 transferred to PVDF membrane (Immuno Blot,Bio-Rad Laboratories) and blocked with 3%
656 nonfat dry milk in TBS-T 0.1%, incubated overnight at 4˚C with primary antibodies (Suppl Table
657 10) and then for one hour with the appropriate secondary antibodies (Suppl Table 10). Proteins
658 were imaged using either the WesternBright Sirius Kit or the WesternBright Quantum Kit
659 (Advansta Inc., San Jose, CA, USA) and the Fusion FX Spectra multimodal imaging platform
660 (Vilber Lourmat, Marne-la-Vallée, France). Quantification of immunoreactive bands was
661 performed using the ImageJ software according to the following pipeline: analyze, gel, select

662 1 lane, plot lanes, manually define the area corresponding to each band, wand tool to quantify
663 each selected area.

664 **Protein extraction for cell secretome analysis**

665 Three independent conditioned media (CM) samples were recovered from SK-N-Be2c Control
666 and sgTWIST1 cells. Once cells reached ~75% of confluence, the medium was replaced with
667 FBS- and phenol red-free DMEM (Gibco) in which cells were incubated for 24 hours. CM were
668 first clarified by three centrifugation steps: 10' at 300 x g; 10' at 2000 x g cells; and 30' at 10000
669 x g at 4°C, and then concentrated using 15 ml Amicon spin filter cartridges (cutoff: 3 kDa,
670 10705884-Merck Millipore, Burlington, MA, USA) by serial addition of 10 ml of CM and
671 centrifugation at 4000 x g until 1.5 ml were left. After dilution in 100 mM Ammonium
672 Bicarbonate buffer to the starting volume, the CM were re-concentrated by centrifugation at
673 4000 x g, and these steps were repeated twice until 0.5 ml were left. Finally, aliquots were
674 snap frozen in liquid nitrogen and used for the LC-MS analysis performed at the Protein
675 Analysis Facility (University of Lausanne, Switzerland). CM were dried in a SpeedVac and then
676 digested according to a modified version of the iST protocol [65]. Pellets were resuspended in
677 50 µl of modified iST buffer (2% sodium deoxycholate, 20mM DTT, 5mM EDTA, 200mM Tris
678 pH 8.6) and heated at 95°C for 5 minutes. 50 µl of 160 mM chloroacetamide (in 10 mM Tris
679 pH 8.6) were then added and cysteines were alkylated for 45 minutes at 25°C in the dark. After
680 1:1 dilution with H2O, samples were adjusted to 3 mM EDTA and digested with 0.5 µg
681 Trypsin/LysC mix (Promega #V5073) for 1h at 37°C, followed by a second 1h digestion with a
682 second, identical aliquot of proteases. To remove sodium deoxycholate, two sample volumes
683 of isopropanol containing 1% trifluoroacetic acid (TFA) were added to the digests, and the
684 samples were directly desalted on a strong cation exchange (SCX) plate (Oasis MCX; Waters
685 Corp., Milford, MA) by centrifugation. After washing with isopropanol/1% TFA, peptides were
686 eluted in 250ul of 80% MeCN, 19% water, 1% (v/v) ammonia.

687 **Mass spectrometry analyses**

688 Tryptic peptides fractions were dried and resuspended in 0.05% TFA, 2% (v/v) acetonitrile, for
689 mass spectrometry analyses. Tryptic peptide mixtures were injected on an Ultimate RSLC
690 3000 nanoHPLC system (Dionex, Sunnyvale, CA, USA) interfaced to an Orbitrap Fusion
691 Tribrid mass spectrometer (Thermo Scientific, Bremen, Germany). Peptides were loaded onto
692 a trapping microcolumn Acclaim PepMap100 C18 (20 mm x 100 µm ID, 5 µm, 100Å, Thermo
693 Scientific) before separation on a reversed-phase custom packed nanocolumn (75 µm ID × 40
694 cm, 1.8 µm particles, Reprosil Pur, Dr. Maisch). A flowrate of 0.25 µl/min was used with a
695 gradient from 4 to 76% acetonitrile in 0.1% formic acid (total time: 65 min). Full survey scans
696 were performed at a 120'000 resolution, and a top speed precursor selection strategy was
697 applied to maximize acquisition of peptide tandem MS spectra with a maximum cycle time of

698 0.6s. HCD fragmentation mode was used at a normalized collision energy of 32%, with a
699 precursor isolation window of 1.6 m/z, and MS/MS spectra were acquired in the ion trap.
700 Peptides selected for MS/MS were excluded from further fragmentation during 60s.

701 **Mass spectrometry data analysis and processing**

702 Tandem MS data were processed by the MaxQuant software (version 1.6.3.4)[66] incorporating
703 the Andromeda search engine[67]. The UniProt human reference proteome database of January
704 2019 was used (73'950 sequences), supplemented with sequences of common contaminants.
705 Trypsin (cleavage at K,R) was used as the enzyme definition, allowing 2 missed cleavages.
706 Carbamidomethylation of cysteine was specified as a fixed modification. N-terminal acetylation
707 of protein and oxidation of methionine were specified as variable modifications. All
708 identifications were filtered at 2% FDR at both the peptide and protein levels with default
709 MaxQuant parameters. After inspection and data QC based on the iBAQ[68] values, the LFQ
710 label-free values[69] were used for protein quantitation. MaxQuant data were further processed
711 with Perseus software[70] for the filtering, log2-transformation, normalization of values and the
712 statistical analyses. After removal of contaminants and reverse hits, intensity values were log2
713 transformed. Only proteins identified by at least two peptides and quantitated in at least all
714 three samples of one condition were retained for further analysis. Missing values were imputed
715 with standard Perseus parameters (normal distribution with width 0.3 and down-shifted by 1.8
716 SD). An unpaired T-test was used to determine significant changes, corrected for FDR with
717 the Benjamini-Hochberg method and a threshold q-value at 0.01. Imputed values were
718 subsequently removed from tables. Gene Ontology functional analysis were performed as
719 previously described in the "Bioinformatics analysis" section, after splitting the lines containing
720 multiple genes references.

721 **Statistical analysis**

722 All statistical analyses were performed using GraphPadPrism 8.3.0 (GraphPad Software Inc.,
723 San Diego, CA, USA). D'Agostino-Pearson normality test was performed for each data set,
724 and depending on data distribution, they were analyzed with unpaired two-tailed parametric t-
725 test or non parametric Mann-Whitney test to compare two different conditions.

726 **Reporting summary.** Further information on research design is available in the Nature
727 Research Reporting Summary linked to this article.

728 Data availability

729 All data generated during this study are included in this article (and its Supplementary
730 Information files). The RNAseq, proteomics and image corresponding datasets can be
731 accessed at the GEO public repository using the accession number GSE160765; at the
732 Proteomics Identifications Database (PRIDE) using the accession number PXD024200; and

733 at the Zenodo repository with the doi: 10.5281/zenodo.4543478, respectively. The RNAseq
734 data of SK-N-Be2c JC1 samples were obtained from GEO, using the accession number
735 GSE80153. The relevant data that support the findings of this study are available from the
736 corresponding author upon reasonable request. Source data are provided with this paper.

737

738 # References

739 1 Maris, J. M. Recent advances in neuroblastoma. *The New England journal of medicine* **362**,
740 2202-2211, doi:10.1056/NEJMra0804577 (2010).
741 2 Brodeur, G. M. Neuroblastoma: biological insights into a clinical enigma. *Nature reviews.*
742 *Cancer* **3**, 203-216, doi:10.1038/nrc1014 (2003).
743 3 Ritenour, L. E., Randall, M. P., Bosse, K. R. & Diskin, S. J. Genetic susceptibility to
744 neuroblastoma: current knowledge and future directions. *Cell and Tissue Research* **372**, 287-
745 307, doi:10.1007/s00441-018-2820-3 (2018).
746 4 Cheung, N. K. & Dyer, M. A. Neuroblastoma: developmental biology, cancer genomics and
747 immunotherapy. *Nature reviews. Cancer* **13**, 397-411, doi:10.1038/nrc3526 (2013).
748 5 Janoueix-Lerosey, I. *et al.* Overall genomic pattern is a predictor of outcome in neuroblastoma.
749 *Journal of clinical oncology : official journal of the American Society of Clinical Oncology* **27**,
750 1026-1033, doi:10.1200/jco.2008.16.0630 (2009).
751 6 Peifer, M. *et al.* Telomerase activation by genomic rearrangements in high-risk neuroblastoma.
752 *Nature* **526**, 700-704, doi:10.1038/nature14980 (2015).
753 7 Ackermann, S. *et al.* A mechanistic classification of clinical phenotypes in neuroblastoma.
754 *Science (New York, N.Y.)* **362**, 1165-1170, doi:10.1126/science.aat6768 (2018).
755 8 Marshall, G. M. *et al.* The prenatal origins of cancer. *Nature reviews. Cancer* **14**, 277-289,
756 doi:10.1038/nrc3679 (2014).
757 9 Le Douarin, N., LeDouarin, N. M. & Kalcheim, C. *The neural crest*. (Cambridge university press,
758 1999).
759 10 Ansieau, S., Morel, A. P., Hinkal, G., Bastid, J. & Puisieux, A. TWISTing an embryonic
760 transcription factor into an oncoprotein. *Oncogene* **29**, 3173-3184, doi:10.1038/onc.2010.92
761 (2010).
762 11 Yeung, K. T. & Yang, J. Epithelial-mesenchymal transition in tumor metastasis. *Molecular*
763 *oncology* **11**, 28-39, doi:10.1002/1878-0261.12017 (2017).
764 12 Franco, H. L., Casasnovas, J., Rodríguez-Medina, J. R. & Cadilla, C. L. Redundant or separate
765 entities?--roles of Twist1 and Twist2 as molecular switches during gene transcription. *Nucleic*
766 *acids research* **39**, 1177-1186, doi:10.1093/nar/gkq890 (2011).
767 13 el Ghouzzi, V. *et al.* Mutations of the TWIST gene in the Saethre-Chotzen syndrome. *Nature*
768 *genetics* **15**, 42-46, doi:10.1038/ng0197-42 (1997).
769 14 Yang, J. *et al.* Twist, a master regulator of morphogenesis, plays an essential role in tumor
770 metastasis. *Cell* **117**, 927-939, doi:10.1016/j.cell.2004.06.006 (2004).
771 15 Valsesia-Wittmann, S. *et al.* Oncogenic cooperation between H-Twist and N-Myc overrides
772 failsafe programs in cancer cells. *Cancer cell* **6**, 625-630, doi:10.1016/j.ccr.2004.09.033 (2004).
773 16 Nozato, M., Kaneko, S., Nakagawara, A. & Komuro, H. Epithelial-mesenchymal transition-
774 related gene expression as a new prognostic marker for neuroblastoma. *International journal*
775 *of oncology* **42**, 134-140, doi:10.3892/ijo.2012.1684 (2013).
776 17 Selmi, A. *et al.* TWIST1 is a direct transcriptional target of MYCN and MYC in neuroblastoma.
777 *Cancer letters* **357**, 412-418, doi:10.1016/j.canlet.2014.11.056 (2015).
778 18 Zeid, R. *et al.* Enhancer invasion shapes MYCN-dependent transcriptional amplification in
779 neuroblastoma. *Nature genetics* **50**, 515-523, doi:10.1038/s41588-018-0044-9 (2018).

19 Zhang, W. *et al.* Comparison of RNA-seq and microarray-based models for clinical endpoint prediction. *Genome Biology* **16**, 133, doi:10.1186/s13059-015-0694-1 (2015).
20 Kocak, H. *et al.* Hox-C9 activates the intrinsic pathway of apoptosis and is associated with spontaneous regression in neuroblastoma. *Cell death & disease* **4**, e586, doi:10.1038/cddis.2013.84 (2013).
21 Eckert, M. A. *et al.* Twist1-induced invadopodia formation promotes tumor metastasis. *Cancer cell* **19**, 372-386, doi:10.1016/j.ccr.2011.01.036 (2011).
22 Balkwill, F. R., Capasso, M. & Hagemann, T. The tumor microenvironment at a glance. *Journal of cell science* **125**, 5591-5596, doi:10.1242/jcs.116392 (2012).
23 Sahai, E. *et al.* A framework for advancing our understanding of cancer-associated fibroblasts. *Nature Reviews Cancer* **20**, 174-186, doi:10.1038/s41568-019-0238-1 (2020).
24 Walker, G. A., Guerrero, I. A. & Leinwand, L. A. Myofibroblasts: molecular crossdressers. *Current topics in developmental biology* **51**, 91-107, doi:10.1016/s0070-2153(01)51003-0 (2001).
25 Mazzoccoli, G. *et al.* A primary tumor gene expression signature identifies a crucial role played by tumor stroma myofibroblasts in lymph node involvement in oral squamous cell carcinoma. *Oncotarget* **8**, 104913-104927, doi:10.18632/oncotarget.20645 (2017).
26 Baum, J. & Duffy, H. S. Fibroblasts and myofibroblasts: what are we talking about? *Journal of cardiovascular pharmacology* **57**, 376-379, doi:10.1097/FJC.0b013e3182116e39 (2011).
27 Tuxhorn, J. A. *et al.* Reactive stroma in human prostate cancer: induction of myofibroblast phenotype and extracellular matrix remodeling. *Clinical cancer research : an official journal of the American Association for Cancer Research* **8**, 2912-2923 (2002).
28 Georgoudaki, A. M. *et al.* Reprogramming Tumor-Associated Macrophages by Antibody Targeting Inhibits Cancer Progression and Metastasis. *Cell Rep* **15**, 2000-2011, doi:10.1016/j.celrep.2016.04.084 (2016).
29 Song, G. *et al.* Direct Reprogramming of Hepatic Myofibroblasts into Hepatocytes In Vivo Attenuates Liver Fibrosis. *Cell Stem Cell* **18**, 797-808, doi:10.1016/j.stem.2016.01.010 (2016).
30 Yeremenko, N. *et al.* Disease-specific and inflammation-independent stromal alterations in spondylarthritis synovitis. *Arthritis Rheum* **65**, 174-185, doi:10.1002/art.37704 (2013).
31 Ansieau, S. *et al.* Induction of EMT by twist proteins as a collateral effect of tumor-promoting inactivation of premature senescence. *Cancer cell* **14**, 79-89, doi:10.1016/j.ccr.2008.06.005 (2008).
32 Zhao, Z., Rahman, M. A., Chen, Z. G. & Shin, D. M. Multiple biological functions of Twist1 in various cancers. *Oncotarget* **8**, 20380-20393, doi:10.18632/oncotarget.14608 (2017).
33 Fang, X. *et al.* Twist2 contributes to breast cancer progression by promoting an epithelial-mesenchymal transition and cancer stem-like cell self-renewal. *Oncogene* **30**, 4707-4720, doi:10.1038/onc.2011.181 (2011).
34 Gasparotto, D. *et al.* Overexpression of TWIST2 correlates with poor prognosis in head and neck squamous cell carcinomas. *Oncotarget* **2**, 1165-1175, doi:10.18632/oncotarget.390 (2011).
35 Mao, Y., Xu, J., Song, G., Zhang, N. & Yin, H. Twist2 promotes ovarian cancer cell survival through activation of Akt. *Oncology letters* **6**, 169-174, doi:10.3892/ol.2013.1316 (2013).
36 Yu, H. *et al.* Twist2 is a valuable prognostic biomarker for colorectal cancer. *World journal of gastroenterology* **19**, 2404-2411, doi:10.3748/wjg.v19.i15.2404 (2013).
37 Beck, B. *et al.* Different levels of Twist1 regulate skin tumor initiation, stemness, and progression. *Cell Stem Cell* **16**, 67-79, doi:10.1016/j.stem.2014.12.002 (2015).
38 Shi, J. *et al.* Disrupting the interaction of BRD4 with diacetylated Twist suppresses tumorigenesis in basal-like breast cancer. *Cancer cell* **25**, 210-225, doi:10.1016/j.ccr.2014.01.028 (2014).
39 Mironchik, Y. *et al.* Twist overexpression induces in vivo angiogenesis and correlates with chromosomal instability in breast cancer. *Cancer research* **65**, 10801-10809, doi:10.1158/0008-5472.Can-05-0712 (2005).

40 Xu, Y. *et al.* Breast tumor cell-specific knockout of Twist1 inhibits cancer cell plasticity, dissemination, and lung metastasis in mice. *Proceedings of the National Academy of Sciences of the United States of America* **114**, 11494-11499, doi:10.1073/pnas.1618091114 (2017).
41 Fu, J. *et al.* The TWIST/Mi2/NuRD protein complex and its essential role in cancer metastasis. *Cell research* **21**, 275-289, doi:10.1038/cr.2010.118 (2011).
42 Bildsoe, H. *et al.* Transcriptional targets of TWIST1 in the cranial mesoderm regulate cell-matrix interactions and mesenchyme maintenance. *Developmental biology* **418**, 189-203, doi:10.1016/j.ydbio.2016.08.016 (2016).
43 Chen, Z. F. & Behringer, R. R. twist is required in head mesenchyme for cranial neural tube morphogenesis. *Genes & development* **9**, 686-699, doi:10.1101/gad.9.6.686 (1995).
44 Yochum, Z. A. *et al.* Targeting the EMT transcription factor TWIST1 overcomes resistance to EGFR inhibitors in EGFR-mutant non-small-cell lung cancer. *Oncogene* **38**, 656-670, doi:10.1038/s41388-018-0482-y (2019).
45 Martin, A. & Cano, A. Tumorigenesis: Twist1 links EMT to self-renewal. *Nature cell biology* **12**, 924-925, doi:10.1038/ncb1010-924 (2010).
46 Schmidt, J. M. *et al.* Stem-cell-like properties and epithelial plasticity arise as stable traits after transient Twist1 activation. *Cell Rep* **10**, 131-139, doi:10.1016/j.celrep.2014.12.032 (2015).
47 Mani, S. A. *et al.* The epithelial-mesenchymal transition generates cells with properties of stem cells. *Cell* **133**, 704-715, doi:10.1016/j.cell.2008.03.027 (2008).
48 Coulon, A. *et al.* Functional sphere profiling reveals the complexity of neuroblastoma tumor-initiating cell model. *Neoplasia* **13**, 991-1004, doi:10.1593/neo.11800 (2011).
49 Winkler, J., Abisoye-Ogunniyan, A., Metcalf, K. J. & Werb, Z. Concepts of extracellular matrix remodelling in tumour progression and metastasis. *Nature communications* **11**, 5120, doi:10.1038/s41467-020-18794-x (2020).
50 Tadeo, I. *et al.* Extracellular matrix composition defines an ultra-high-risk group of neuroblastoma within the high-risk patient cohort. *British journal of cancer* **115**, 480-489, doi:10.1038/bjc.2016.210 (2016).
51 Chakraborty, S. *et al.* Twist1 promotes heart valve cell proliferation and extracellular matrix gene expression during development in vivo and is expressed in human diseased aortic valves. *Developmental biology* **347**, 167-179, doi:10.1016/j.ydbio.2010.08.021 (2010).
52 García-Palmero, I. *et al.* Twist1-induced activation of human fibroblasts promotes matrix stiffness by upregulating palladin and collagen α1(VI). *Oncogene* **35**, 5224-5236, doi:10.1038/onc.2016.57 (2016).
53 Shamir, E. R., Coutinho, K., Georgess, D., Auer, M. & Ewald, A. J. Twist1-positive epithelial cells retain adhesive and proliferative capacity throughout dissemination. *Biology open* **5**, 1216-1228, doi:10.1242/bio.019703 (2016).
54 Wang, S. *et al.* Up-regulation of PCOLCE by TWIST1 promotes metastasis in Osteosarcoma. *Theranostics* **9**, 4342-4353, doi:10.7150/thno.34090 (2019).
55 Puissant, A. *et al.* Targeting MYCN in neuroblastoma by BET bromodomain inhibition. *Cancer Discov* **3**, 308-323, doi:10.1158/2159-8290.CD-12-0418 (2013).
56 Dubois, S. G. *et al.* Lung metastases in neuroblastoma at initial diagnosis: A report from the International Neuroblastoma Risk Group (INRG) project. *Pediatric blood & cancer* **51**, 589-592, doi:10.1002/pbc.21684 (2008).
57 Chen, Q., Wang, J., Liu, W. N. & Zhao, Y. Cancer Immunotherapies and Humanized Mouse Drug Testing Platforms. *Transl Oncol* **12**, 987-995, doi:10.1016/j.tranon.2019.04.020 (2019).
58 Seeger, R. C. *et al.* Morphology, growth, chromosomal pattern and fibrinolytic activity of two new human neuroblastoma cell lines. *Cancer research* **37**, 1364-1371 (1977).
59 Biedler, J. L. & Spengler, B. A. A novel chromosome abnormality in human neuroblastoma and antifolate-resistant Chinese hamster cell lives in culture. *J Natl Cancer Inst* **57**, 683-695, doi:10.1093/jnci/57.3.683 (1976).
60 Shalem, O. *et al.* Genome-scale CRISPR-Cas9 knockout screening in human cells. *Science (New York, N.Y.)* **343**, 84-87, doi:10.1126/science.1247005 (2014).

884 61 Sanjana, N. E., Shalem, O. & Zhang, F. Improved vectors and genome-wide libraries for CRISPR
885 screening. *Nature methods* **11**, 783-784, doi:10.1038/nmeth.3047 (2014).
886 62 Flahaut, M. *et al.* Aldehyde dehydrogenase activity plays a Key role in the aggressive
887 phenotype of neuroblastoma. *BMC Cancer* **16**, 781, doi:10.1186/s12885-016-2820-1 (2016).
888 63 Carr, J. *et al.* High-resolution analysis of allelic imbalance in neuroblastoma cell lines by single
889 nucleotide polymorphism arrays. *Cancer genetics and cytogenetics* **172**, 127-138,
890 doi:10.1016/j.cancergencyto.2006.08.012 (2007).
891 64 Joseph, J. M. *et al.* In vivo echographic evidence of tumoral vascularization and
892 microenvironment interactions in metastatic orthotopic human neuroblastoma xenografts. *Int*
893 *J Cancer* **113**, 881-890, doi:10.1002/ijc.20681 (2005).
894 65 Kulak, N. A., Pichler, G., Paron, I., Nagaraj, N. & Mann, M. Minimal, encapsulated proteomic-
895 sample processing applied to copy-number estimation in eukaryotic cells. *Nature methods* **11**,
896 319-324, doi:10.1038/nmeth.2834 (2014).
897 66 Cox, J. & Mann, M. MaxQuant enables high peptide identification rates, individualized p.p.b.-
898 range mass accuracies and proteome-wide protein quantification. *Nature biotechnology* **26**,
899 1367-1372, doi:10.1038/nbt.1511 (2008).
900 67 Cox, J. *et al.* Andromeda: a peptide search engine integrated into the MaxQuant environment.
901 *Journal of proteome research* **10**, 1794-1805, doi:10.1021/pr101065j (2011).
902 68 Schwanhäusser, B. *et al.* Global quantification of mammalian gene expression control. *Nature*
903 **473**, 337-342, doi:10.1038/nature10098 (2011).
904 69 Cox, J. *et al.* Accurate proteome-wide label-free quantification by delayed normalization and
905 maximal peptide ratio extraction, termed MaxLFQ. *Molecular & cellular proteomics : MCP* **13**,
906 2513-2526, doi:10.1074/mcp.M113.031591 (2014).
907 70 Tyanova, S. *et al.* The Perseus computational platform for comprehensive analysis of
908 (prote)omics data. *Nature methods* **13**, 731-740, doi:10.1038/nmeth.3901 (2016).

909

910 **Acknowledgements**

911 We thank Dr. Manfredo Quadroni (Protein Analysis Facility, University of Lausanne) and his
912 team for their help with the secretome analysis. Dr Jessica Dessimoz (Histology Core Facility
913 of the EPFL) and Janine Horlbeck (Mouse Pathology Facility) for their help with the IHC and
914 tissue staining. Dr Julien Marquis (Lausanne Genomics Technologies Facility) for his technical
915 advice in the targeted sequencing analysis of the indels in TWIST1 gene. This work was
916 supported by grants from Kinderkrebsforschung Schweiz (to A.M.M.), the Novartis Foundation
917 for Medical-Biological Research (to A.M.M.), the Hubert Gouin Association (to A.M.M.), and
918 the FORCE foundation (to A.M.M. and R.R.).

919 **Author contributions**

920 M.V.S. performed all major experimental work, with the technical help of K.B.B., M.V.S. and
921 A.M.M. analyzed the data, prepared figures and drafted the manuscript, J.M.J and N.J.
922 performed *in vivo* xenograft implantations, K.N.A. constructed the LentiCRISPR v2-sgTWIST1
923 vectors, J.Y.S. provided the TMA., H.S. performed the TMA analysis and the interpretation of
924 the related data, A.P. provided help in the TMA analysis, V.P. conducted the bioinformatics
925 analysis, N.R. performed pathological analyses of the xenografts, R.R. interpreted the data

926 and edited the manuscript, A.M.M. designed, supervised the study and coordinated
927 experiments. All authors read, commented and approved the final manuscript.

928 **Competing interests**

929 The authors declare no competing interests.

930 **Correspondence** and requests for materials should be addressed to A.M.M.

931 # Figures and Figure Legends

932

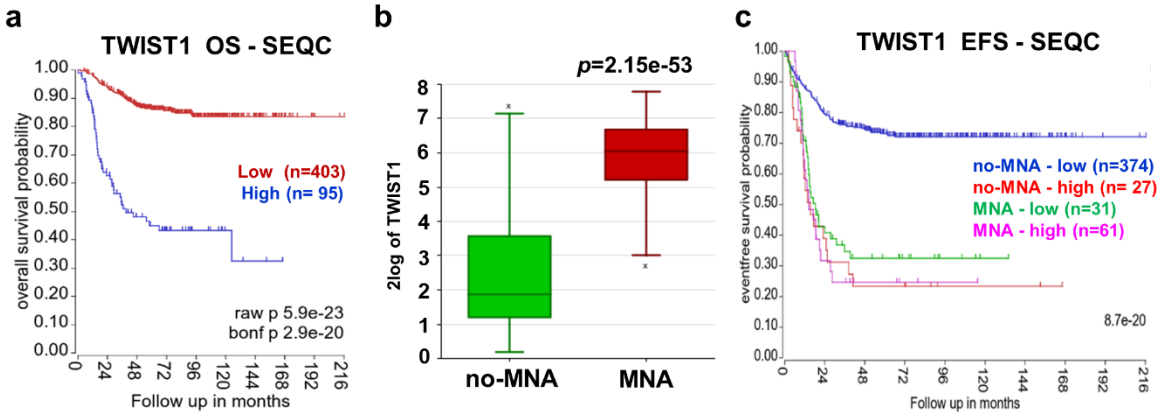

933

934

935 **Figure 1. TWIST1 RNA expression is associated with poorer outcome of NB patients.** (**a-**
936 **c**) Analysis of TWIST1 expression in the SEQC dataset of primary NB tumors. (**a**) Kaplan-
937 Meier OS curve associated with TWIST1 expression. Expression cutoff: 44.441. (**b**) Box-and-
938 whisker plots of TWIST1 expression in tumors with MNA or without MNA (no-MNA). (**c**)
939 Kaplan-Meier EFS curves showing the stratification of patients according to MYCN status and
940 TWIST1 expression (high or low).

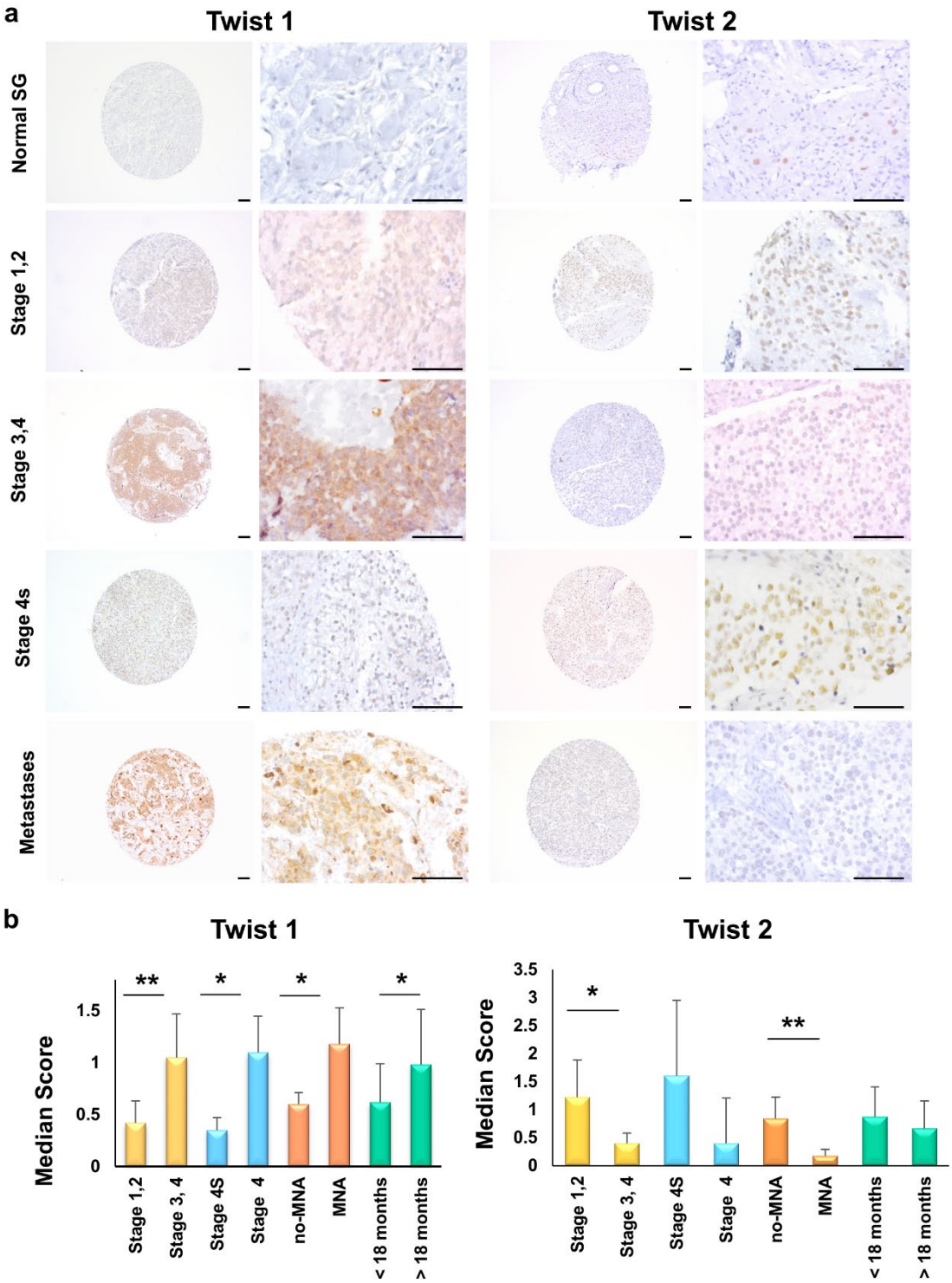

941

942

943 **Figure 2. TWIST1 and TWIST2 display an opposite protein expression profile in a NB**
944 **tissue microarray.** (**a**) TWIST1 and TWIST2 protein expression were analyzed by IHC using
945 a NB TMA containing 97 tumor sections: 72 primary tumors, 25 matched metastases and 44
946 matched control normal tissues (i.e. SG). Representative images of TWIST1 and TWIST2 IHC

947 staining are shown for each indicated category. Magnification 100x (left panels) and 400x (right
948 panels); scale bares=100 μm. (**b**) Bar graphs showing the median scores (ms) ± SD of TWIST1
949 and TWIST2 IHC staining for different comparisons (see Table 1). Statistical analysis was done
950 using parametric Student's t-test.

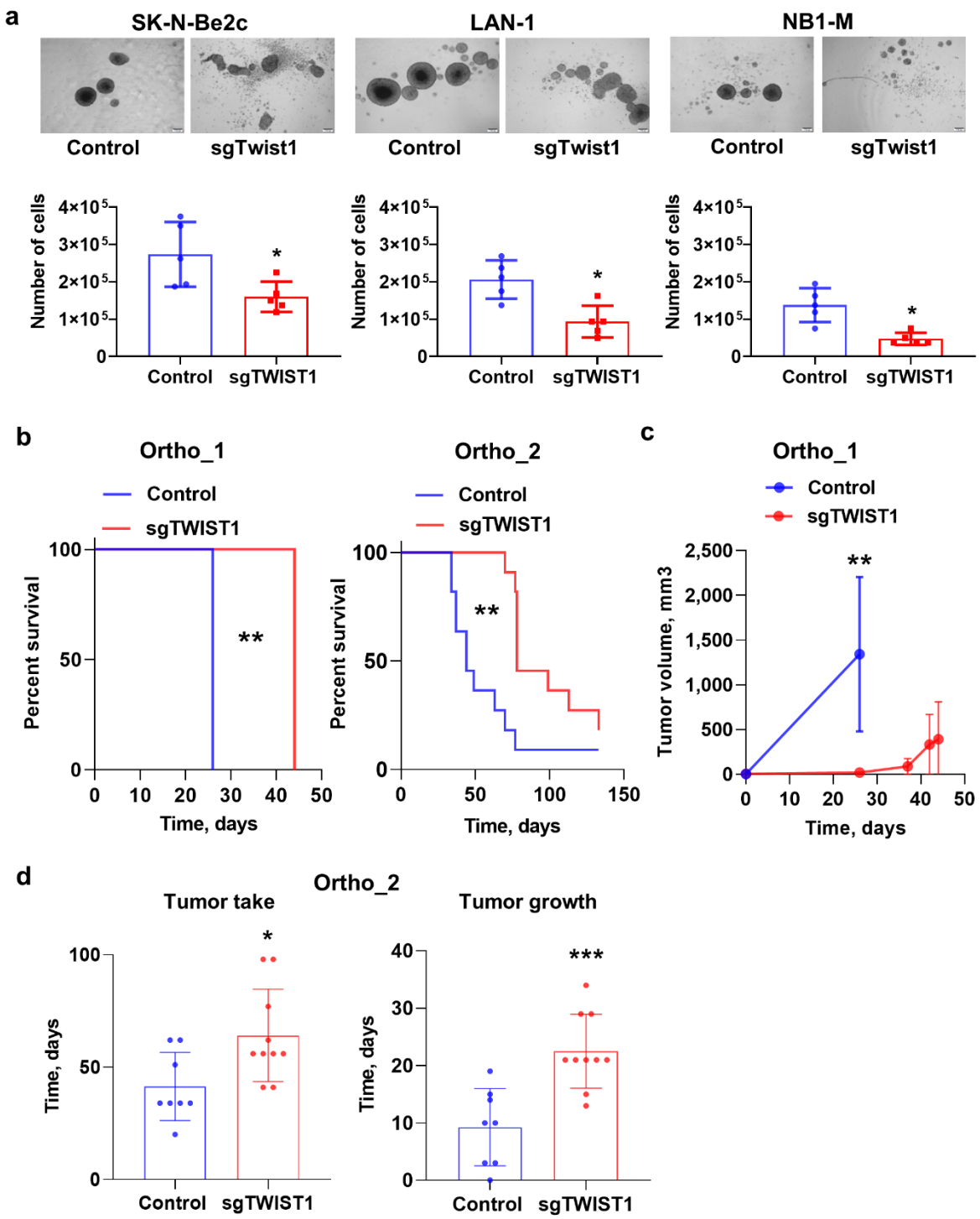

Figure 3. TWIST1 KO reduces the neurosphere forming capacities of NB cells *in vitro* and the tumor growth capacities of SK-N-Be2c cells *in vivo*. (**a**) Upper panel: representative images (scale bar 200 µm) showing the size and shape of primary neurospheres of Control and sgTWIST1 NB cells after 7 days in culture. Lower panel: the numbers of cells obtained after dissociation of Control and sgTWIST1 primary neurospheres are plotted in bare graphs as individual values for each independent experiments and mean ± SD (n=5 experiments performed in duplicates). Mann Whitney test: *p=0.0317 for SK-N-Be2c;

959 *p=0.0159 for LAN-1 and NB1-M. (**b**) Kaplan-Meier survival curves of athymic Swiss nude mice
960 implanted with SK-N-Be2C-Control or -sgTWIST1 cells. Mice were sacrificed once tumors
961 reached the volume of 1000 mm^3 and 500 mm^3 for ortho_1 and ortho_2 experiments,
962 respectively. Tumor take: ortho_1: 100% (6/6) in the Control group, 66.66% (4/6) in the
963 sgTWIST1 group; ortho_2: 89% (8/9) in the Control group, 83% (10/12) in the sgTWIST1
964 group. Median survival in the Control vs sgTWIST1 group: 26 vs 44 days for ortho_1
965 (**p=0.0027); 49 vs 78 days for ortho_2 (**p=0.0016). Gehan-Breslow-Wilcoxon test. (**c**)Tumor
966 growth (mean tumor volumes ± SD) for ortho_1 experiment. Multiple t-test (Holm-Sidak,
967 α=0.05, without assuming a consistent SD): **p=0.0037. (**d**) Time for tumor initiation (left) and
968 tumor growth (right) in the ortho_2 experiment (mean days ± SD). Tumor initiation correspond
969 to the number of days required to measure an AG volume > 10 mm^3 (mean Control: 41.38
970 days, sgTWIST1: 64.10 days, *p=0.0192). Time for tumor growth was calculated as the
971 number of days at sacrifice minus the number of days for tumor initiation (mean Control: 9.25
972 days, sgTWIST1: 22.50 days, ***p=0.0006). Unpaired t-test.

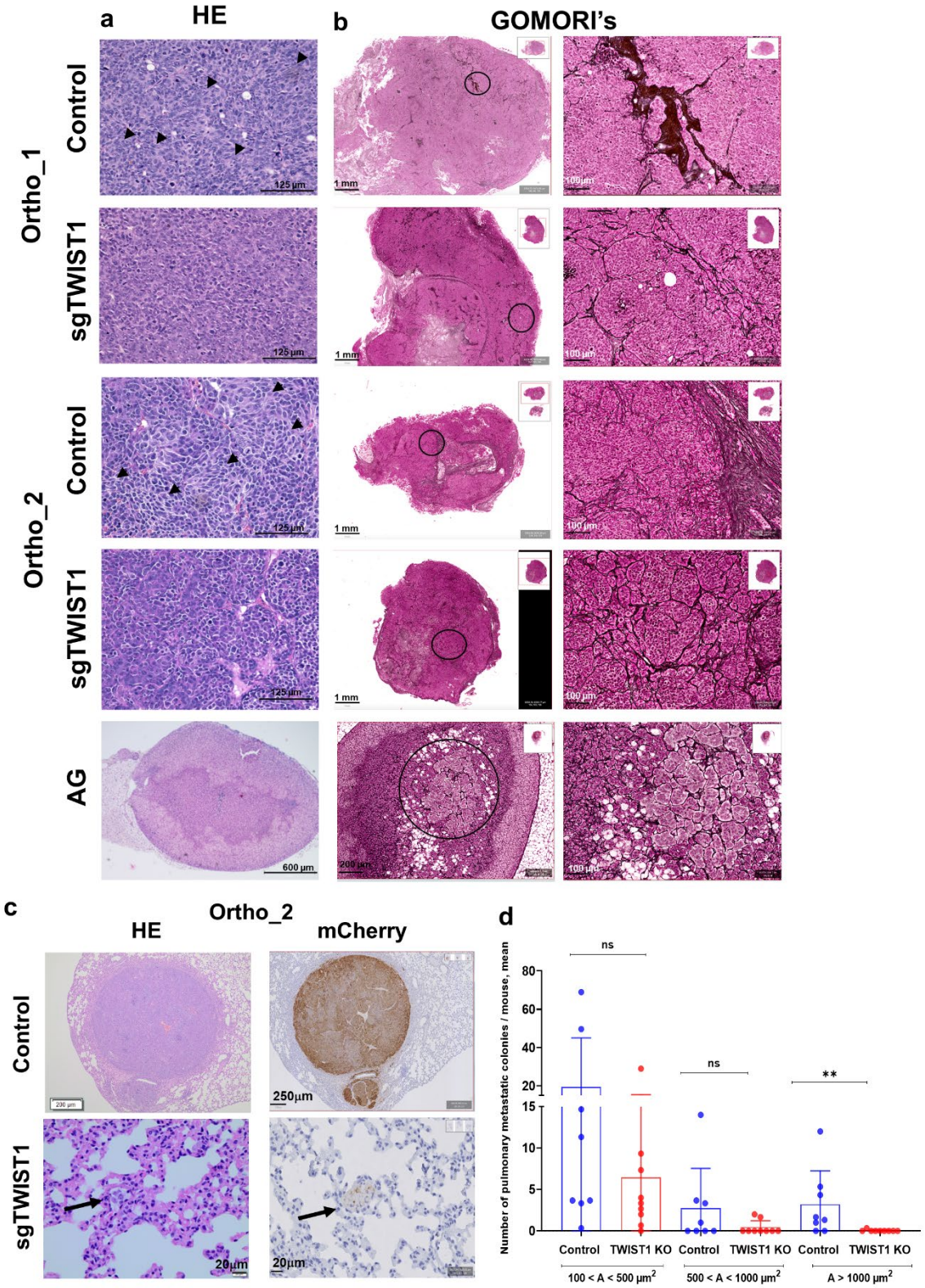

Figure 4. TWIST1 KO produces tumor with a less aggressive phenotype and impairs the formation of the intrapulmonary macrometastases. (**a**) Representative images of H&E staining of ortho tumors and AG. H&E staining of both ortho-derived tumors depicted cells in

977 control tissues separated by thin fibro-vascular septs having irregular size and shape; no
978 discernable/scarce cytoplasm; one or few prominent nucleoli; spindle-shaped cells with
979 fusiform nuclei (black arrow) that tended to have a fascicular organization. Conversely,
980 sgTWIST1 tumor cells were portrayed by a more regular size and shape (round to oval) with
981 only slight irregularities, finely granular ("salt-and-pepper") chromatin, small nucleoli and
982 moderate/more discernible cytoplasm (scale bar: 125 μm for tumors; 600μm for AG). (**b**)
983 Representative images of Gomori's staining showing the architecture of the collagen
984 III/reticulin fibers in ortho tumors and AG. Left panels: large views of tumor and AG sections;
985 scale bars: 1 mm and 200 μm, respectively. Right panels: zoomed view of the region
986 highlighted by a black circle, scale bars: 100 μm for both tumors and AG. (**c**) H&E and anti-
987 mCherry staining for pulmonary metastases detection in the lungs of ortho_2 mice. Upper
988 panel: representative images of Control mice; lower panel: pictures of the unique
989 macrometastasis detected in sgTWIST1 group of mice. (**d**) Quantification of metastases
990 detected by IHC anti-mCherry within the parenchyma (intrapulmonary) of mice. Of note, no
991 metastases were detected at the pleural surface and/or in mediastinal soft tissue
992 (peripulmonary). Data are plotted in a bar graph showing individual values and mean ± SD for
993 micrometastases (100-500 μm^2: p=0.2257; 500-1000 μm^2: p=0.1855) and for
994 macrometastases (>1000 μm^2, **p= 0.0041). Mann-Whitney test. Percent of mice with
995 macrometastases = 75% in the Control group; 10% in the sgTWIST1 group.

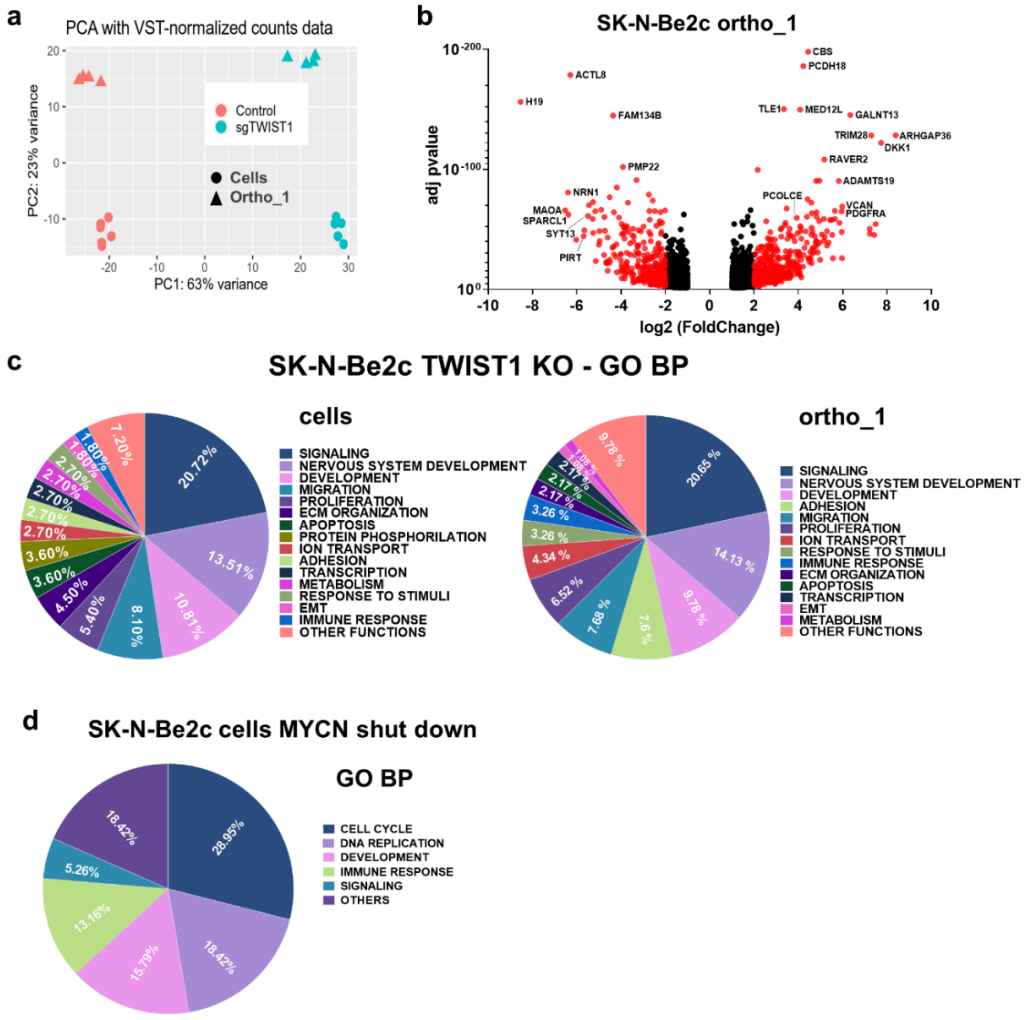

Figure 5. The biological pathways deregulated by TWIST1 KO are distinct from those mediated by MYCN shut down. (**a**) PCA samples repartition using the VST-normalized counts. PCA1 and PCA2 are 63% and 23% of total variation, respectively. (**b**) Volcano plots showing the distribution of the DE genes according to FC (log2) and adj *p* value between the SK-N-Be2c-Control and –sgTWIST1 ortho_1-derived xenografts. Genes with False Discovery Rate (FDR) < 0.05 and absolute value (av) of log2(FC) ≥ 1 were considered as DE; in red genes with av of log2(FC) ≥2, in black genes with av of log2(FC) ≥ 1 and <2. Positive and negative x-values represent genes either up- or down-regulated by TWIST1, respectively. (**c**). Illustration of the biological processes gene sets found enriched by GO analyses (GO BP) in the DE genes following TWIST1 KO for both SK-N-Be2c cells (left panel) and ortho_1 tumors (right panel). Data are reported as the repartition (in %) of the diverse pathways identified with a FDR < 0.01 (n=111 for cells, n=92 for tumors). (**d**) Illustration of the GO BP gene sets found enriched in the DE genes in SK-N-Be2c cells upon JC1-medited MYCN shutdown. RNAseq data of SK-N-Be2c cells treated with JC1 during 24h or DMSO as control were uploaded (GSE80154, see Methods) (Zeid et al.). Genes with False Discovery Rate (FDR) < 0.05 and

1012 absolute value (av) of log2(FC) ≥ 1 were considered as DE. Data are reported as the repartition
1013 (in %) of the diverse pathways identified with a FDR < 0.01 (n=38).

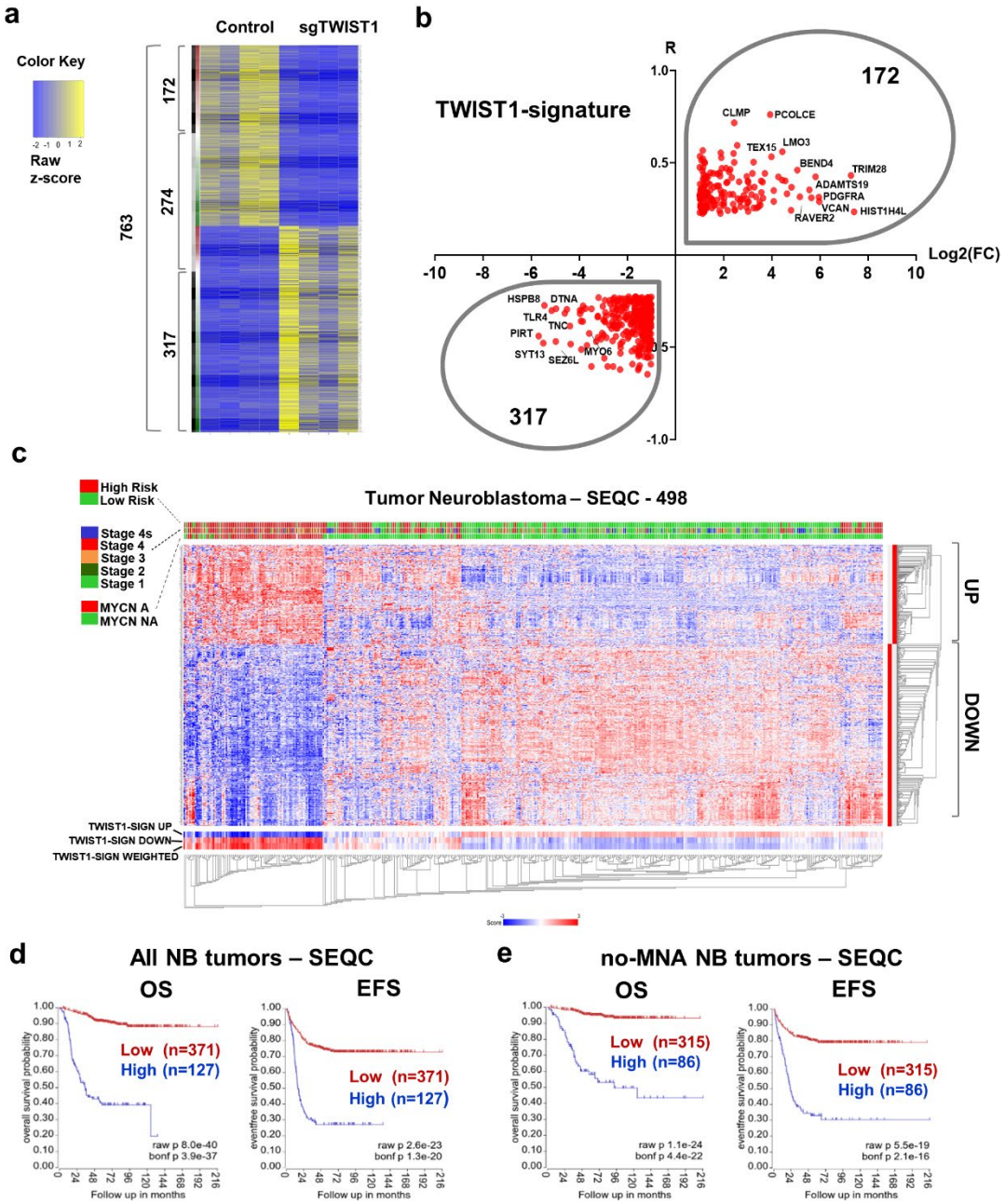

Figure 6. **Identification of a TWIST1-associated gene signature correlating with poor prognosis in NB**. (**a**) Heatmap showing 763 common genes either correlated or anti-correlated with TWIST1 in NB patients and DE in the ortho_1 tumors. The binary side color bar going from green to red indicates DE genes anti-correlated (R<-0.225, green) or correlated (R>0.225, red) with TWIST1 in the SEQC dataset; the black bar shows the genes that have both FC and R values either positive or negative representing the TWIST1-signature, and the grey bar the genes that have opposite FC and R values (not included in the signature). (**b**) Volcano plot showing the distribution of the 489 genes of the TWIST1-signature according to their log2(FC) in SK-N-Be2c ortho_1 tumors and R values in the SEQC dataset . (**c**) Heatmap

1047 hierarchical clustering showing different expression pattern relative to TWIST1-signature
1048 genes generated using the R2 Platform (http://r2.amc.nl). Columns represent patients
1049 annotated in the SEQC cohort; the 489 genes are clustered hierarchically along the left y-axis.
1050 Clinical criteria taken into consideration (risk groups, tumor stages, and MYCN amplification
1051 status) are indicated on the top by color codes. The heat map indicates in red, blue and white
1052 a high, low and a medium level of gene expression (z-score), respectively. The blue-white-red
1053 color bars depicted at the bottom of the heatmap represent the z-score of TWIST1_Up and
1054 TWIST1_Down gene sub-lists of the signature, as well as for the z-score of the whole signature
1055 (weighted). (**f-g**) Kaplan-Meier OS and EFS survival curves according to the expression level
1056 of the TWIST1-signature in both the complete SEQC dataset (**f**) and in the sub-cohort of
1057 patients without MNA (no-MNA) (**g**). Expression cutoff: 0.20 (**f**) and -0.05 (**g**).

1058

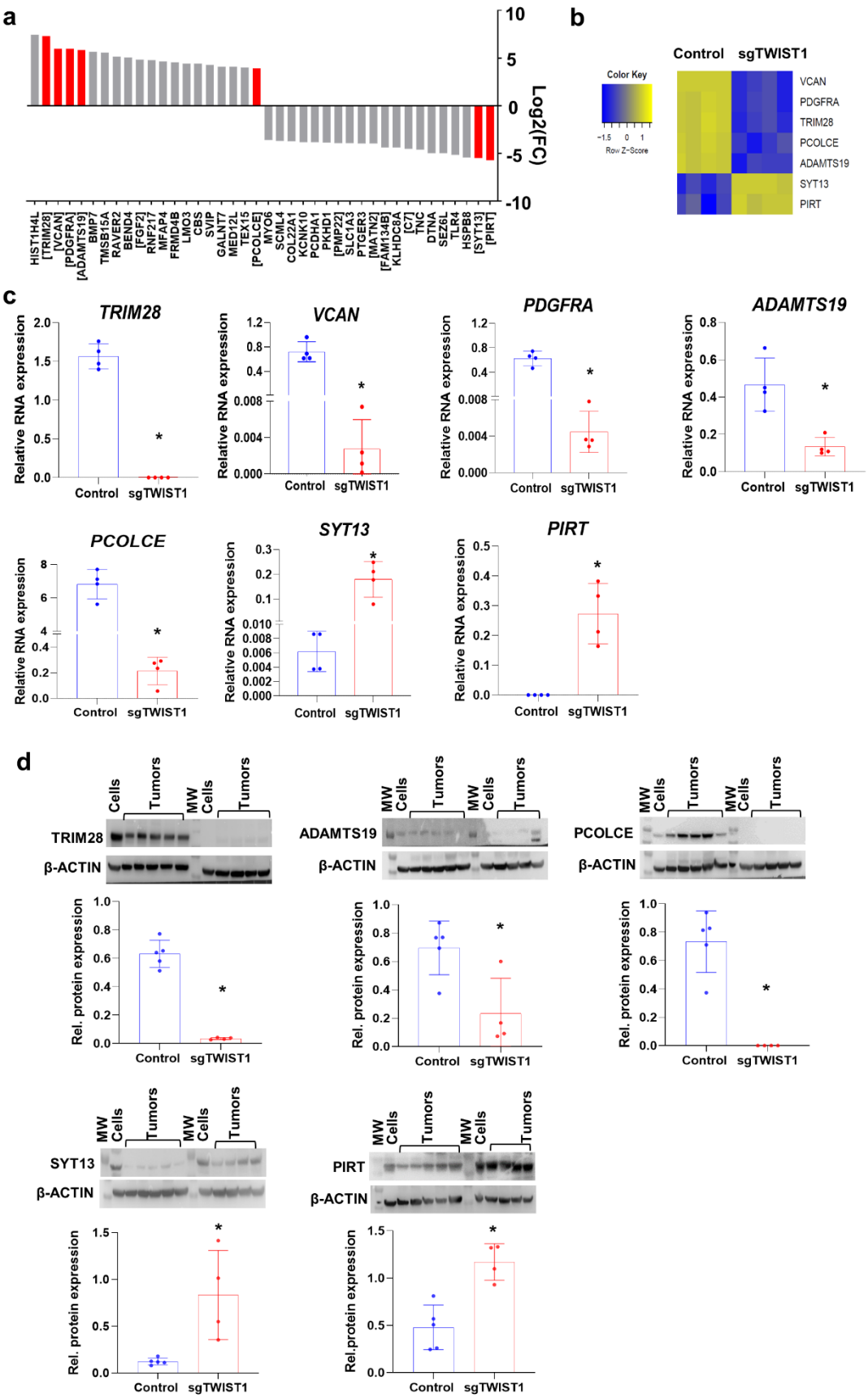
a
Log2(FC)
HIST1H4L
[TRIM28]
[VCAN]
[PDGFRA]
[ADAMTS19]
BMP7
TMSB15A
RAVER2
BEND4
[FGF2]
RNF217
MFAP4
FRMD4B
LMO3
CBS
SVIP
GALNT7
MED12L
TEX15
[PCOLCE]
MYO6
SCML4
COL22A1
KCNK10
PCDHA1
PKHD1
[PMP22]
SLC1A3
PTGER3
[MATN2]
[FAM134B]
KLHDC8A
[C7]
TNC
DTNA
SEZ6L
TLR4
HSPB8
[SYT13]
[PIRT]
b
Control
sgTWIST1
Color Key
Row Z-Score
VCAN
PDGFRA
TRIM28
PCOLCE
ADAMTS19
SYT13
PIRT
c
TRIM28
VCAN
PDGFRA
ADAMTS19
PCOLCE
SYT13
PIRT
Relative RNA expression
Control
sgTWIST1
d
Cells
Tumors
MW Cells
TRIM28
ADAMTS19
PCOLCE
SYT13
PIRT
β-ACTIN
Rel. protein expression
Control
sgTWIST1

1059

1060 **Figure 7. Validation of TWIST1-mediated deregulation of selected genes belonging to**
1061 **the TWIST1 signature in the ortho_1 tumors.** (**a**) Bar plots showing the distribution of the
1062 top 20 up- and 20 down-regulated genes of the TWIST1 signature ordered according to their
1063 log2(FC). In red, genes that were selected for the validation at both RNA and protein levels.
1064 Gene names in brackets indicate up-regulated genes involved in the EMT process, TME
1065 organization, proliferation and apoptosis; and down-regulated genes that are known to be
1066 tumor suppressor genes or associated with good prognosis in NB. (**b**) Heatmap showing the
1067 relative RNA expression (z-score) determined by RNAseq of the selected genes in ortho_1
1068 tumors. (**c**) RNA expression levels of the TWIST1 target genes relative to the reference gene
1069 *HPRT1* in the ortho_1 tumors analyzed by RT-qPCR are plotted as individual values with mean
1070 ± SD. Control n= 6 ; sgTWIST1 n= 4. Mann Whitney test: *p=0.0286 for all comparisons. (**d**)
1071 Upper panel: Immunoblotting for TRIM28, ADAMTS19, PCOLCE, ADAMTS19, SYT13 and
1072 PIRT (β-ACTIN as the loading control); lower panel: densitometric quantifications of
1073 immunoreactive band densities. Expression relative to β-ACTIN were plotted as individual data
1074 with mean ± SD. Control n= 5; sgTWIST1n= 4 . Mann Whitney test: *p= 0.0317 for ADAMTS19;
1075 *p= 0.0159 for the other proteins.

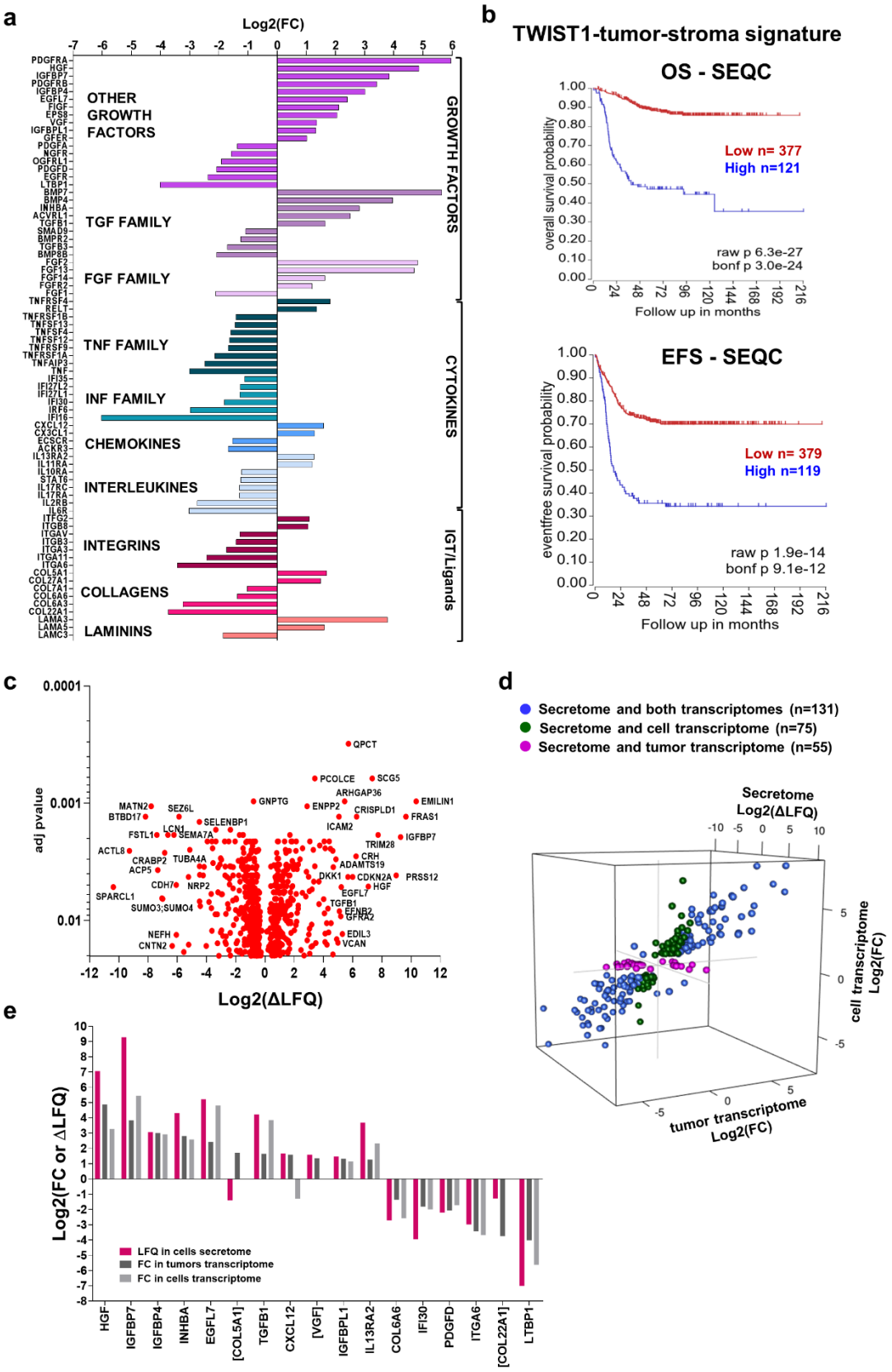

Figure 8. **Identification of a TWIST1-mediated-tumor-stroma signature associated with poor outcome in NB.** (**a**) Bar plot illustrating of the 77 DE genes representing the TWIST1-

1079 tumor-stroma signature in SK-N-Be2c ortho_1 tumors. Genes were classified according to their
1080 log2(FC) in three main categories: growth factors (including the TGF and FGF families).
1081 cytokines (TNF and INF families, chemokines and interleukins), and integrins and their ligands
1082 (ITG, collagens and laminins). (**b**) Kaplan-Meier OS and EFS curves of NB patients of the
1083 SEQC dataset according to the expression level of the TWIST1-tumor-stroma signature.
1084 Expression cutoff for both curves: 0.10. (**c**) Volcano plot showing the distribution of the DE
1085 protein secreted by SK-N-Be2c cells according to the delta label-free quantification (ΔLFQ =
1086 LFQ SK-N-Be2c Control – LFQ SK-N-Be2c sgTWIST1) intensities (Log2) and the adjusted *p*
1087 values with an FDR ≤ 0.02 analyzed by LC-MS/MS (n= 3 biological replicates for each group).
1088 (**d**) 3D scatterplot showing DE terms in the cell secretome in common with the tumor
1089 transcriptome (magenta, n=55), the cell transcriptome (green, n=75), or both transcriptomes
1090 (blue, n=131). (**e**) Bar plot showing the terms commonly deregulated between the TWIST1-
1091 tumor-stroma signature and both the cell transcriptome and secretome. Names in brackets are
1092 for terms found to be DE in the secretome but not in the transcriptome of cells.

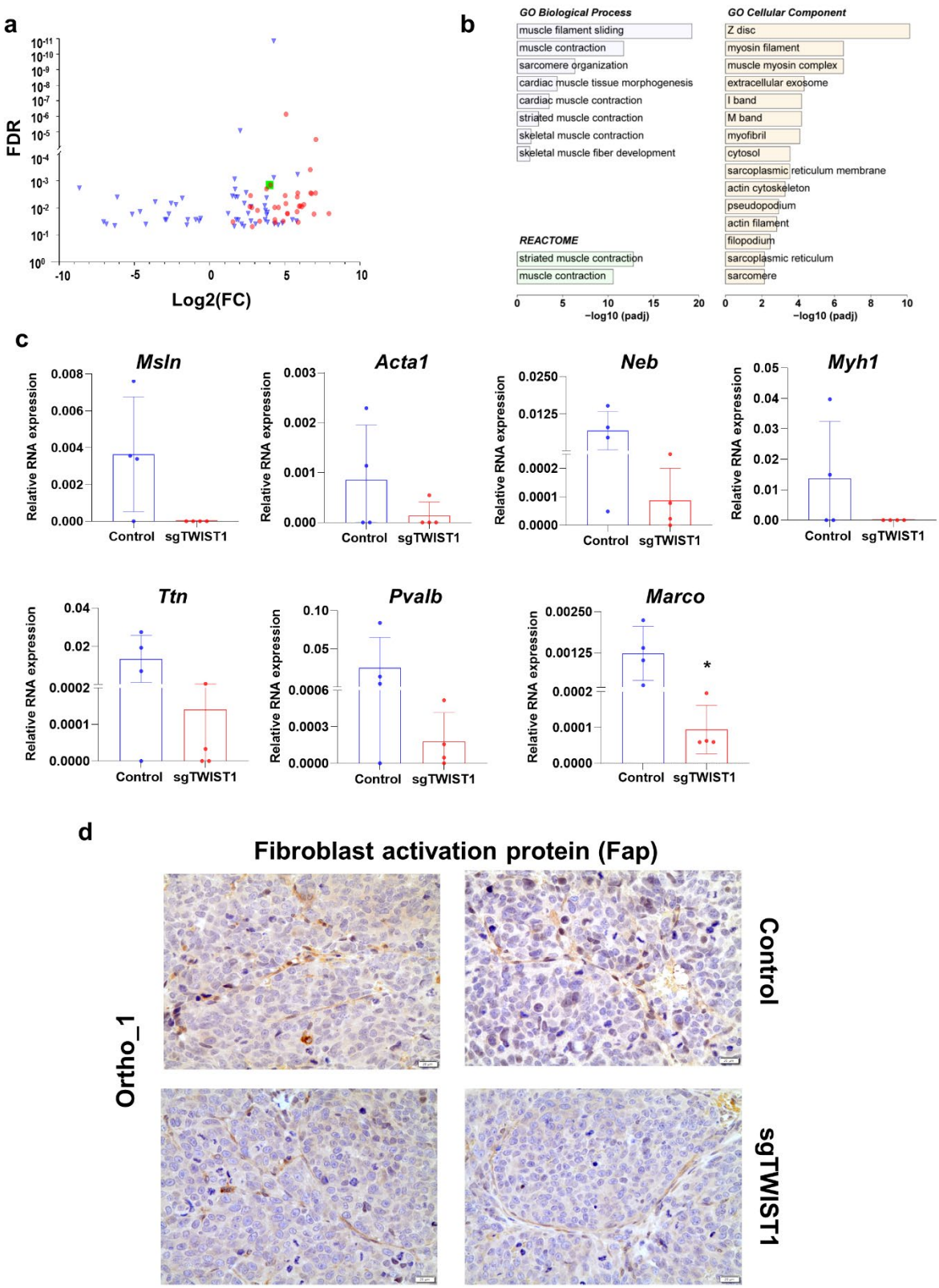

Figure 9. **Identification of a TWIST1-associated myofibroblast signature**. (**a**) Volcano plots showing the distribution of the DE gene identified in SK-N-Be2c-Control and –sgTWIST1 tumor stroma of ortho_1 xenografts relative to their log2(FC) and adjusted *p* value (FDR). Genes with FDR < 0.05 and absolute value (av) of log2(FC) ≥ 0.5 were considered as DE. Genes identified

as the Myofibroblast signature are indicated in red (n=36). The green square is for the gene *Marco*. (**b**) Bar graph showing the biological processes, cellular components and REACTOME pathways identified by GO analysis of the 89 DE genes of the murine stroma, listed according to their adjusted *p* value. (**c**) mRNA expression levels of the selected myofibroblast genes and Marco relative to β-actin as by RT-qPCR. Data are plotted as individual values with mean ± SD. Mann Whitney test: *p= 0.0286. Ortho_1 Control and sgTWIST1 tumors: n=4. (**d**) IHC for the cancer-associated fibroblast marker Fibroblasts Activation Protein (FAP) on ortho_1 Control and sgTWIST1 tumors. Representative images of FAP positive cells characterized by spindle or fusiform morphologies and haphazardly arranged are shown (400x, scale bar: 20 μm).

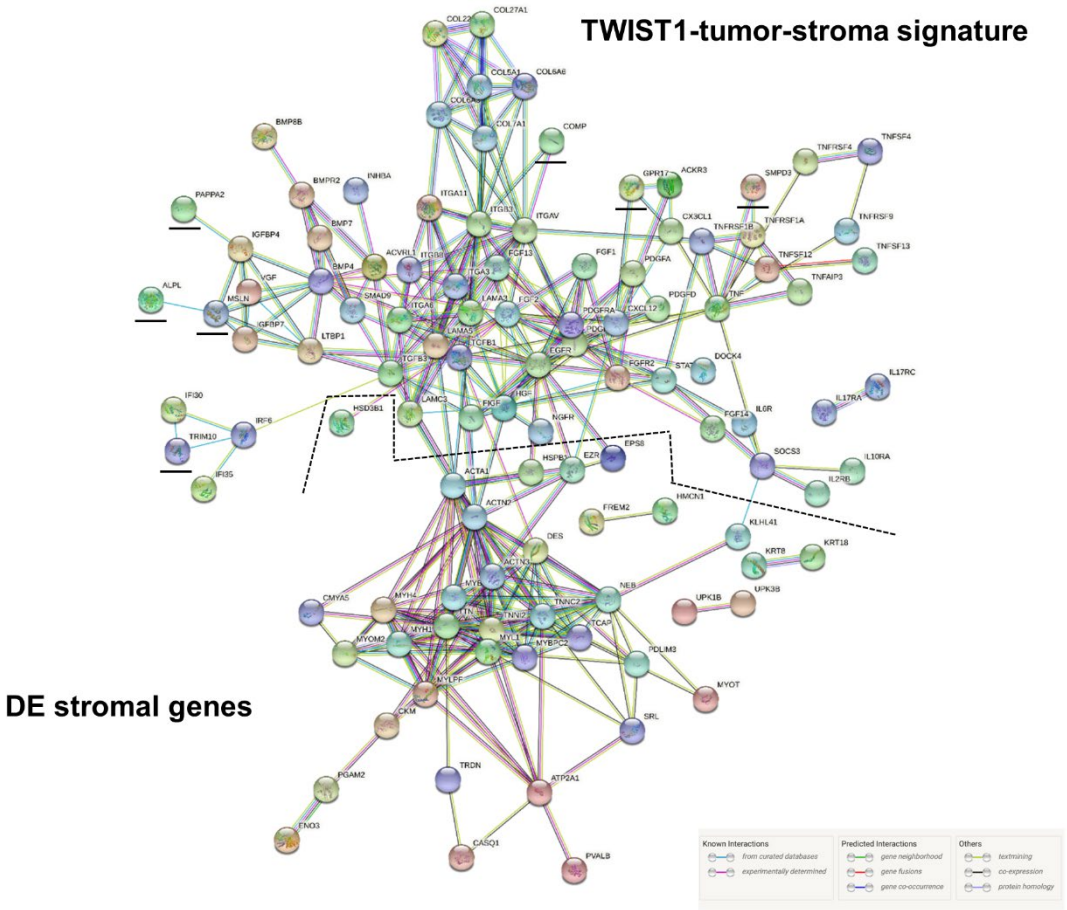

Figure 10. **PPI network for the TWIST1-associated tumor-stroma signature and the DE stromal genes.** Analysis of the protein-protein interactions between the TWIST1-tumor-stroma signature (n= 77 genes) and the DE murine stromal genes (n=89)**.** Direct (physical) as well as indirect (functional) interactions analyzed using the String website. All the basic and advanced default settings have been kept but the minimum required interaction score, that has been changed in high confidence (0.7); and the network display options, hiding the disconnected nodes in the network. PPI enrichment *p* value: <1.0^{e}-16. Murine stromal genes clustering with the TWIST1 tumor-stroma signature are underlined in black.

1123

	Total n (%)	TWIST1				TWIST2			
		Positive tissue n (%)	Median score	SD	*p* value	Positive tissue n (%)	Median score	SD	*p* value
Sample Type									
Primary tumor	72	52 (72)	0.84	0.78		30 (42)	1.1	0.87	
Metastasis	25	19 (76)	0.95	0.74		8 (32)	0.31	0.3	
Lymph node	22	18 (82)	1.05	0.72		7 (32)	0.3	0.53	
Liver	3	1 (33)	0.66	0.31		1 (33)	0.75	0.35	
Control normal tissu = SG	44	0 (0)	0	0		20 (45)	0.58	0.53	
Age (mo)									
Median (range)									
<18 months	27	8 (30)	0.62	0.37	*p =0.045	16 (59)	0.87	0.53	ns
≥ 18 months	45	33 (73)	0.98	0.53		26 (58)	0.66	0.49	
INSS stage									
1	12 (16.7)	4 (33)	0.41	0.19		4 (33)	1.08	0.98	
2	6 (8.3)	3 (50)	0.41	0.24		3 (50)	1.5	0.52	
3	13 (13.8)	10 (77)	1.03	0.48		7 (54)	0.37	0.2	
4	36 (50)	30 (83)	1.1	0.35	*p =0.04	13 (36)	0.4	0.18	ns
4S	5 (6.9)	2 (40)	0.35	0.12		3 (60)	1.6	1.35	
1, 2	18 (25)	7 (39)	0.42	0.21	**p <0.01	7 (39)	1.22	0.67	*p= 0.045
3, 4	49 (68)	40 (82)	1.05	0.42		20 (41)	0.4	0.18	
MYCN amplification									
MNA	13	11 (85)	1.18	0.35	*p= 0.02	3 (23)	0.17	0.12	**p< 0.01
no-MNA	47	11 (23)	0.6	0.11		22 (47)	0.84	0.38	

1124

1125 **Table 1.** Composition of the TMA and expression of TWIST1 and TWIST2 in NB primary
1126 tumors, metastases and control tissues. SG: sympathetic ganglia, INSS: International
1127 Neuroblastoma Staging System, n: number of cases. Median score means average tumor
1128 score, as established by semi-quantitative analysis of the immunostaining. Student's t-test:
1129 *p<0.05, **p<0.01, p≥0.05 were considered as not significant (ns).

1130

1131

1132

1133

1134

Gene description	Gene	log2FC	padj	
Desmin	Des	1.5436	0.0326	**Myofibroblast markers**
Mesothelin	Msln	5.0785	7.2658E-07	
Actin, alpha 1, skeletal muscle	Acta1	6.6873	0.0004	
Actinin alpha 2	Actn2	5.0222	0.0035	
Actinin alpha 3	Actn3	5.8876	0.0337	
Myosin binding protein C, slow-type	Mybpc1	6.7193	0.0028	**Sarcomeric thin filament**
Nebulin	Neb	4.8947	0.0307	
Nebulin-related anchoring protein	Nrap	7.0611	3.0668E-05	
Troponin C2, fast	Tnnc2	6.9370	0.0169	
Troponin I, skeletal, fast 2	Tnni2	5.0686	0.0069	
Xin actin-binding repeat containing 2	Xirp2	5.1731	0.0162	
Cardiomyopathy associated 5	Cmya5	3.8505	0.0337	
Myosin binding protein C, fast-type	Mybpc2	5.9514	0.0087	
Myosin, heavy polypeptide 1, skeletal muscle, adult	Myh1	6.0248	0.0084	
Myosin, heavy polypeptide 4, skeletal muscle, adult	Myh4	6.7812	0.0029	
Myosin, light polypeptide 1	Myl1	5.8567	0.0028	**Sarcomeric thick filament**
Myosin light chain, phosphorylatable, fast skeletal muscle	Mylpf	6.2615	0.0075	
Myomesin 2	Myom2	4.3271	0.0096	
Myotilin	Myot	4.3341	0.0273	
Myelin regulatory factor	Myrf	2.7196	0.0035	
Titin-cap	Tcap	5.8251	0.0039	
Titin	Ttn	5.1708	0.0161	
Parvalbumin	Pvalb	7.9325	0.1618	**Calcium ion-binding protein**

1135

1136

1137 **Table 2.** Summary of myofibroblast markers and principal muscle structure-specific genes
1138 identified in the myofibroblast signature of ortho_1 tumors (labeled in red in **Fig. 9a)** with their
1139 log2(FC) and adjusted *p* values.

1140

1141

1142

1143

Supplementary Figure 1

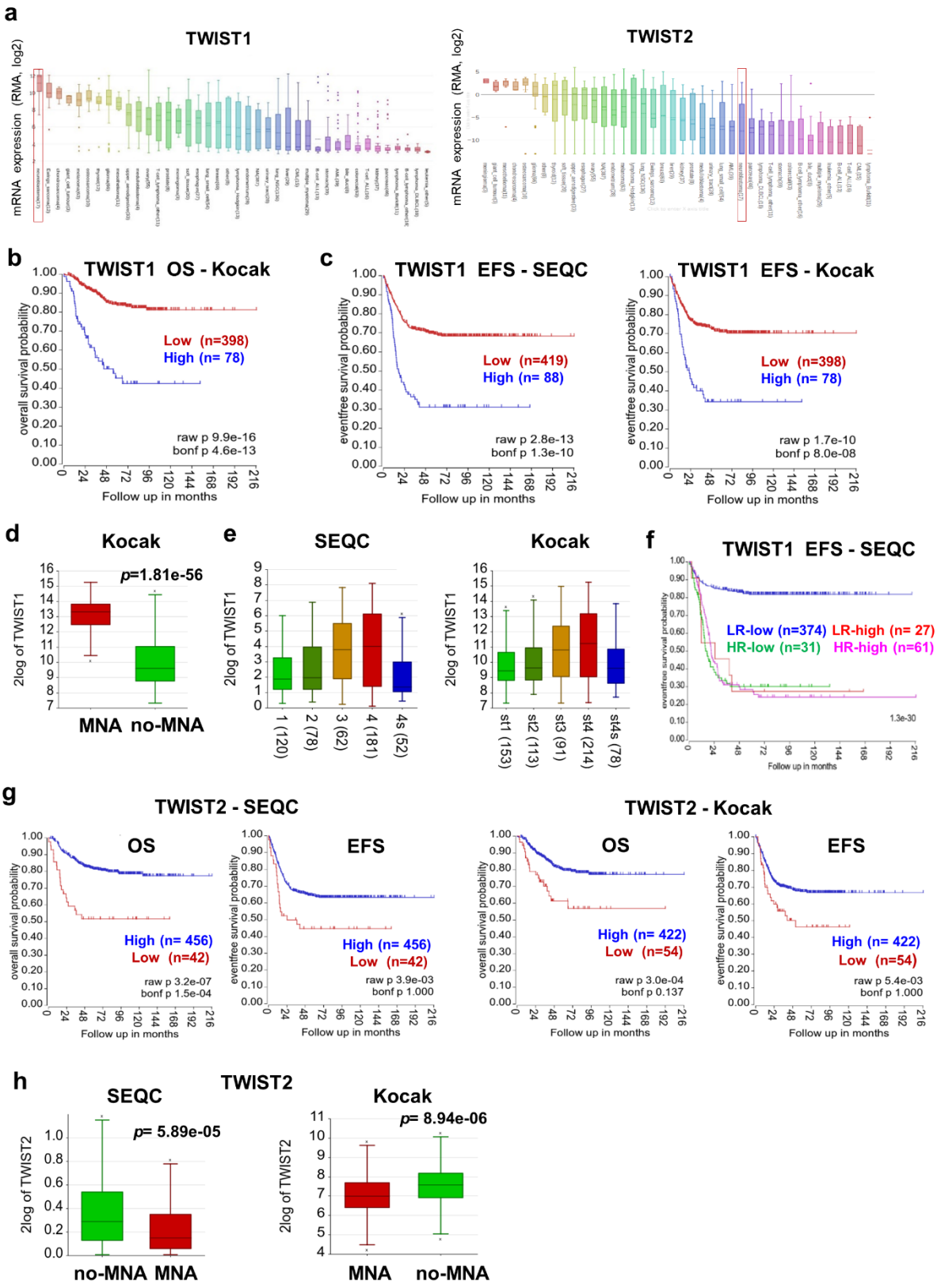

Supplementary Fig. 1. **TWIST1 and TWITS2 RNA expression in NB cells and tumors**. (**a**) Box plot showing the mRNA expression levels of TWIST1 (left) and TWIST2 (right) in a panel of 40 cancer cell lines in the CCLE database. The numbers in the brackets correspond to the numbers of cell lines per tumor types. (**b**) Kaplan-Meier OS curve associated with TWIST1 expression in the Kocak dataset of primary NB tumors (expression cutoff = 6701.9) (n=476 with survival data). (**c**) EFS associated with TWIST1 expression in the SEQC (left panel, expression cutoff: 44.441) and Kocak (right panel, expression cutoff = 6701.9) datasets. (**d-e**) Box-and-whisker plots of TWIST1 expression in MNA and no-MNA tumors (**d**); and in tumors with distinct INSS stages in the indicated datasets (**e**). (**f**) Kaplan-Meier EFS curves showing the stratification of patients of the SEQC dataset according to the risk classification (high-risk: HR; low-risk: LR) and TWIST1 expression (high or low). (**g**) OS and EFS according to TWIST2 expression in the SEQC (left panels, expression cutoff: 1010) and Kocak (right panels, expression cutoff: 86.0) datasets. (**h**) Box-and-whisker plots of TWIST2 expression in no-MNA and MNA tumors in the SEQC and Kocak datasets.

20 **Supplementary Figure 2**

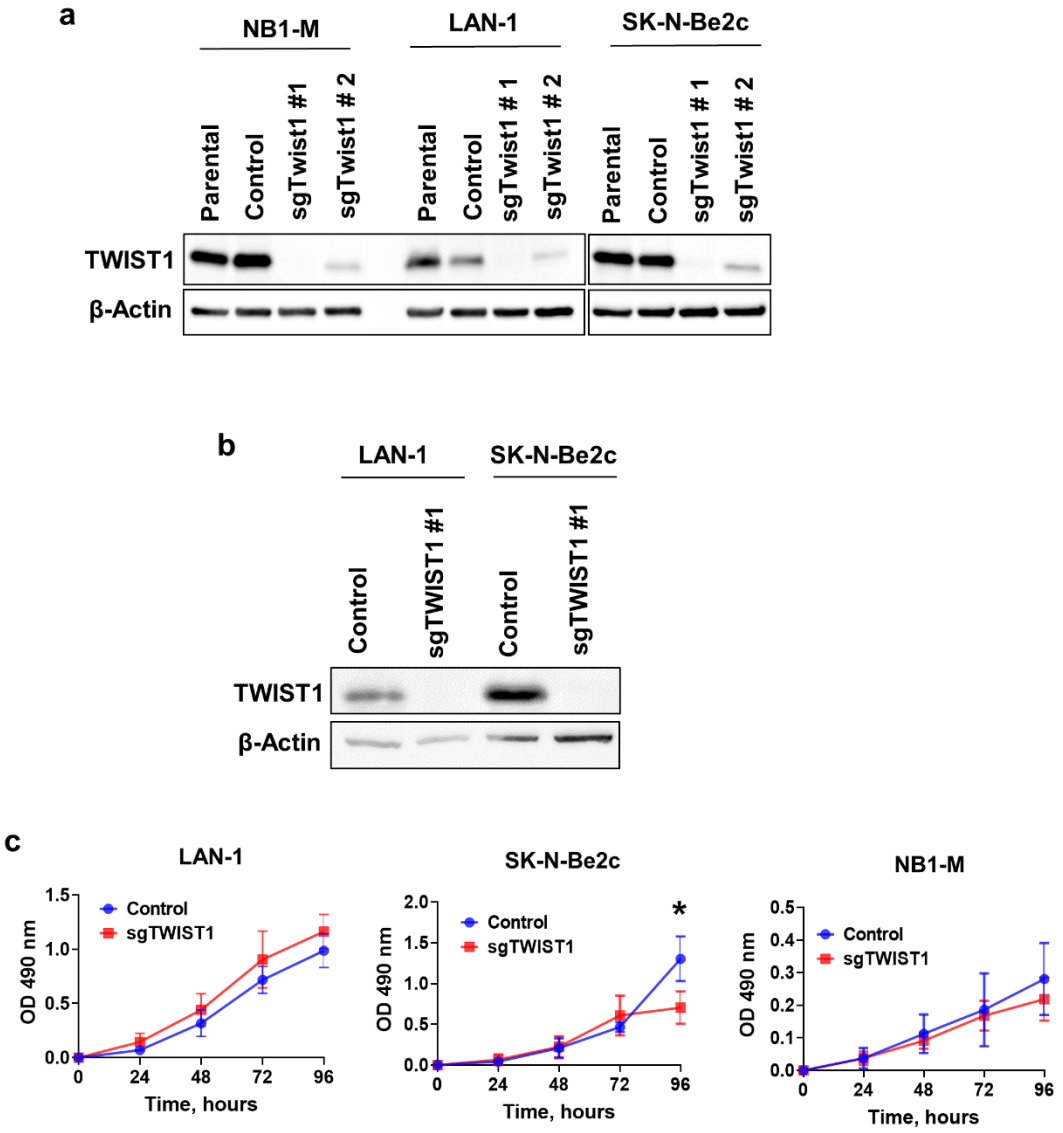

21

22

23 **Supplementary Fig. 2. Validation of the CRISPR/Cas9-mediated TWIST1 KO and its**
24 **impact on NB cell proliferation *in vitro***. (**a**) Immunoblotting for the detection of TWIST1
25 protein expression and β-actin (as the loading control) in the bulk populations of NB cells before
26 (Parental) and after the lentiviral infection: Control vector, sgTWIST1#1 (sgTWIST1, from now
27 on) and sgTWIST1#2. (**b**) TWIST1 protein expression in the LAN-1 and SK-N-Be2c pool of
28 clones for Control and sgTWST1 (see Matherial&Methods). (**c**) Cell proliferation of Control and
29 sgTWST1 NB cell lines measured by MTS/PMS assay from 24h to 96h. Mean OD 490nm ±
30 SD of three (SK-N-Be2c) and four (LAN-1 and NB1-M) independent experiments performed in
31 quadruplicates are shown. Statistical analysis was done using the Holm-Sidak multiple t-test
32 (α=0.05), without assuming a consistent SD. *p= 0.0376 in SK-N-Be2c.

33

34 **Supplementary Figure 3**

35

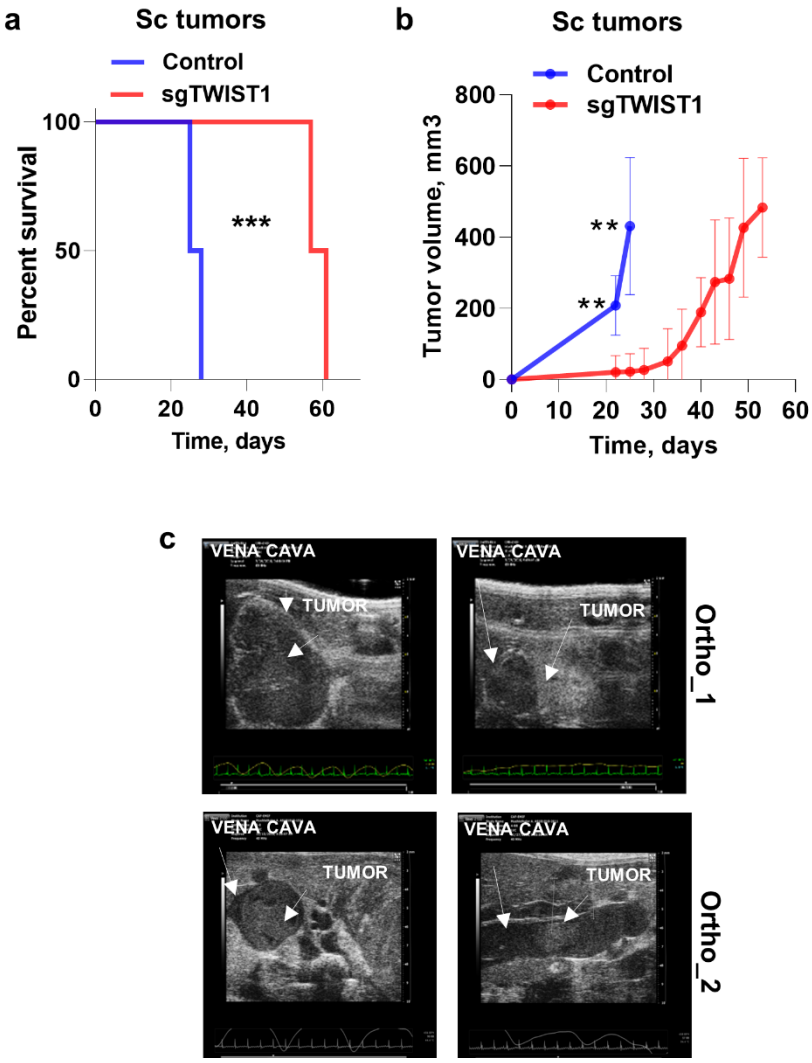

36

37 **Supplementary Fig. 3. TWIST1 KO diminishes the tumor growth and invasive capacities**
38 **of SK-N-Be2c cells.** (**a**) Kaplan-Meier survival curve of mice implanted subcutaneously with
39 SK-N-Be2c-Control or -sgTWIST1 cells. Mice were sacrificed once tumors reached
40 approximately 700 mm^3. Tumor take: 100% (5/5) in both groups. Median survival in the Control
41 vs sgTWIST1 groups: 26.5 vs 59 days. Gehan-Breslow-Wilcoxon test: ***p=0.0002. (**b**) Tumor
42 growth curve for the sc experiment. Data are plotted as the mean tumor volume ± SD. Mann-
43 Whitney t-test: **p= 0.0079 at both 22 and 25 days. (**c**) Representative ultrasound images of
44 tumor cell intravasation in the vena cava of 2 distinct ortho_1 and ortho_2 Control mice.

45

46 **Supplementary Figure 4**

47

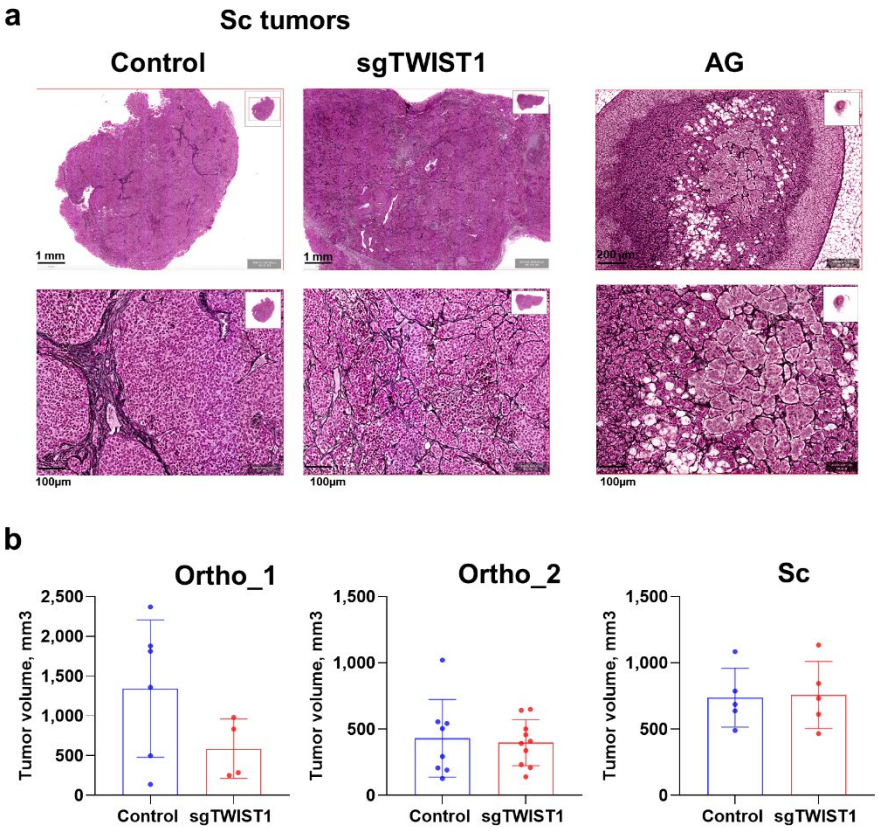

48

49

50 **Supplementary Fig. 4. TWIST1 KO affects the the Collagen III/reticulin network**
51 **organization.** (**a**) Representative images of Gomori's staining showing the ECM architecture
52 of Control and sgTWIST1 sc tumors (scale bars: top 1mm; bottom 100µm) as compared to the
53 normal AG (scale bars: top 200 µm; bottom 100 µm). (**b**) Graphs illustrating the mean tumor
54 volumes at sacrifice ± SD. Ortho_1: mean Control= 1343 mm^3, n=6; sgTWIST1= 587 mm^3,
55 n=4; Mann-Whitney test: p= 0.257. Ortho_2*:* mean Control= 430 mm^3, n= 8; sgTWIST1= 397
56 mm^3, n=10; unpaired t-test: p= 0.. *SC*: mean Control: 737 mm^3, n=5; sgTWIST1= 757 mm^3,
57 n=5; Mann-Whitney: p>0.999.

58

59 **Supplementary Figure 5**

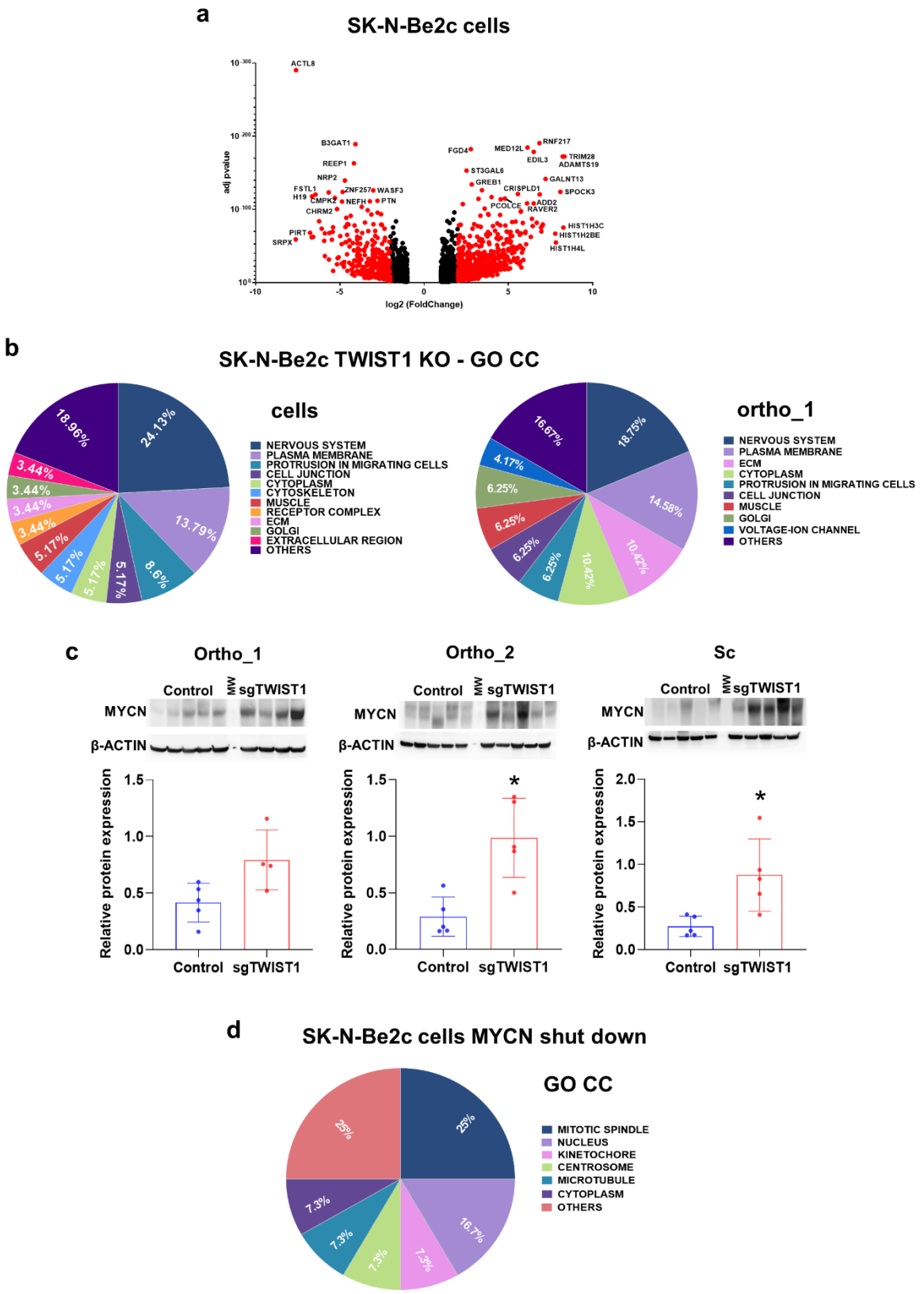

60

61 **Supplementary Fig. 5. Distinct transcriptional programs are affected upon TWIST1 KO**
62 **and MYCN shut down.** (**a**) Volcano plots showing the distribution of the gene expression fold

changes and adjusted *p* value for the DE genes in SK-N-Be2c-Control versus SK-N-Be2c–sgTWIST1 cells. Genes with False Discovery Rate (FDR) < 0.05 and absolute value (av) of log2(FC) ≥ 1 were considered as DE; in red genes with av of log2(FC) ≥2, in black genes with av of log2(FC) ≥ 1 and <2. Positive and negative x-values represent genes either up or down-regulated by TWIST1 respectively. (**b**)**.** Illustration of the cellular components gene sets found enriched by GO analyses (GO CC) in the DE genes following TWIST1 KO for both SK-N-Be2c cells (left panel) and ortho_1 tumors (right panel). Data are reported as the repartition (in %) of the diverse pathways identified with a FDR < 0.01 (n=58 for cells, n=48 for tumors). (**c**) Immunoblotting for MYCN protein and β-actin as control (upper panel) and densitometric quantification of MYCN expression relative to β-ACTIN (lower panel) in SK-N-Be2c-derived tumors of the 3 *in vivo* experiments. Expressions relative to β-ACTIN were plotted as individual data with mean ± SD. Mann Whitney test. **p*= 0.0159 in ortho_2 and sc. Ortho_1: n= 5 Control; n= 4 sgTWIST1; ortho_2 and sc: n= 5 Control; n= 5 sgTWIST1. (**d**) Illustration of the GO CC gene sets found enriched in the DE genes of SK-N-Be2c cells upon JC1-medited MYCN shutdown. RNAseq data of SK-N-Be2c cells treated with JC1are during 24h or DMSO as control were uploaded (GSE80154, see Methods) (Zeid et al.). Genes with False Discovery Rate (FDR) < 0.05 and absolute value (av) of log2(FC) ≥ 1 were considered as DE. Data are reported as the repartition (in %) of the diverse pathways identified with a FDR < 0.01 (n=24).

82 # Supplementary Figure 6

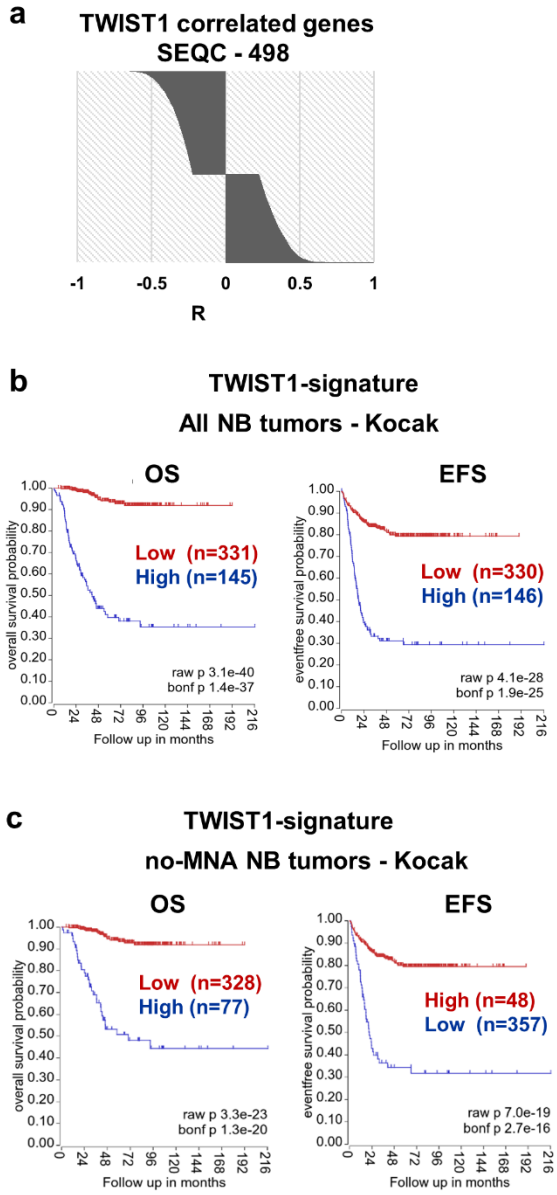

83

84 **Supplementary Fig. 6. Identification of a TWIST1-signature associated with poor**
85 **survival in NB.** (**a**) Illustration of the 7737 genes correlated with TWIST1 expression in the
86 SEQC dataset of NB primary tumors with the repartition of the R values. Source probeset:
87 NM_000474; R *p* value cutoff: 0.01; Corr. multiple testing: Bonferroni. (**b-c**) Kaplan-Meier OS
88 and EFS survival curves associated with the expression of the TWIST1-signature both in the
89 complete Kocak cohort with survival data (n=476) (**b**) and in the no-MNA sub-cohort (n=405)
90 (**c**). Expression cutoff: 0.03 for both curves.

91

92 **Supplementary Figure 7**

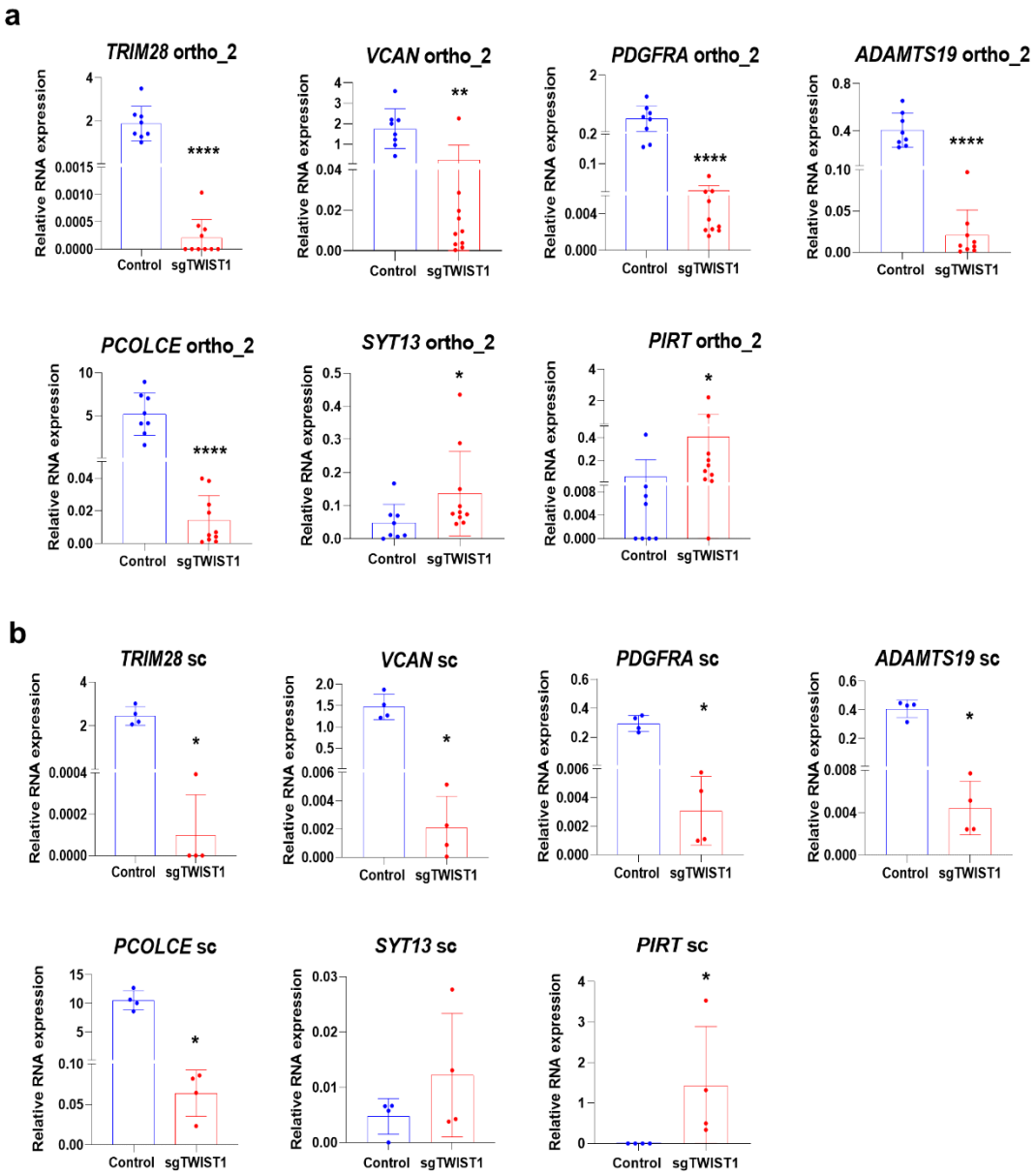

93

94

95 **Validation of TWIST1-mediated deregulation of selected TWIST1 target genes at the**
96 **RNA level in SK-N-Be2c-derived tumors**. (**a-b**) mRNA expression levels of the selected
97 TWIST1 target genes relative to *HPRT1* analyzed by RT-qPCR are plotted as individual values
98 with mean ± SD for the indicated *in vivo* experiments**.** Numbers of tumors analyzed for ortho_2
99 (**a**): Control n= 8, sgTWIST1 n= 10; and for sc (**b**): Control n= 4, sgTWIST1 n= 4. Statistical
100 analysis was performed using Mann Whitney test for all genes but *PCOLCE in* ortho_2
101 experiment (unpaired t-test: ****p<0.0001). Ortho_2: *TRIM28*: ****p=0.0001 2; *VCAN*:
102 **p=0.0021; *PDGFRA* and *ADAMTS19*: ****p=0.0001; *PIRT*: *p=0.0146; *SYT13*: *p=0.0266;
103 sc: *TRIM28*: *p=0.; *VCAN*, *PDGFRA*, *ADAMTS19* and *PIRT*: *p=0.0286; SYT13: *p=0.0266.

Supplementary Figure 8

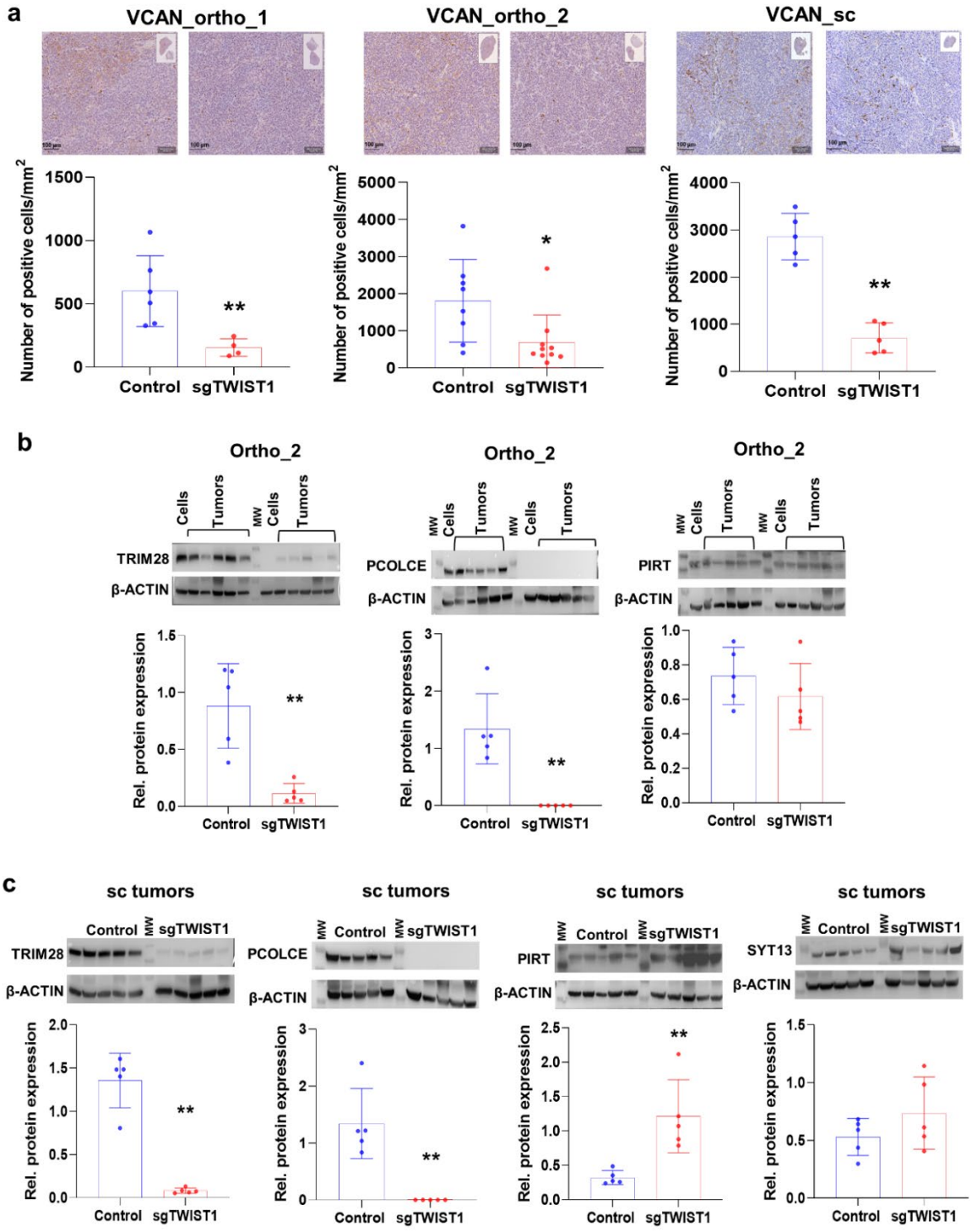

Supplementary Fig. 8. Analysis of the protein expression levels of selected TWIST1 target genes in SK-N-Be2c-derived tumors. (**a**) Upper panels: representative images of IHC for VCAN in the indicated tumors (scale bar =100 μm); lower panels: quantification of VCAN

staining (Qpath software on total area of each section). Mann-Whitney: ortho_1:**p=0.0095, n=6 Control and n=4 sgTWIST1; ortho_2: *p= 0.0155, n=8 Control and n=10 sgTWIST1; sc: **p=0.0079, n=5 Control and n=5 sgTWIST1. (**b-c**). Relative protein expression as determined by immunoblotting for the selected genes in the ortho_2 (**b**) and the sc (**c**) tumors. Upper panel: Representative images of immunoblotting for TRIM28, PCOLCE, PIRT and SYT13 (β-ACTIN as the control); MW: molecular weight; lower panel: densitometric quantifications of immunoreactive band densities. Expressions relative to β-ACTIN were plotted as individual data with mean ± SD. Mann Whitney test: **p=0.0079 for all comparisons. Ortho_2 and sc: n=5 Control and n=5 sgTWIST1.

120 **Supplementary Figure 9**

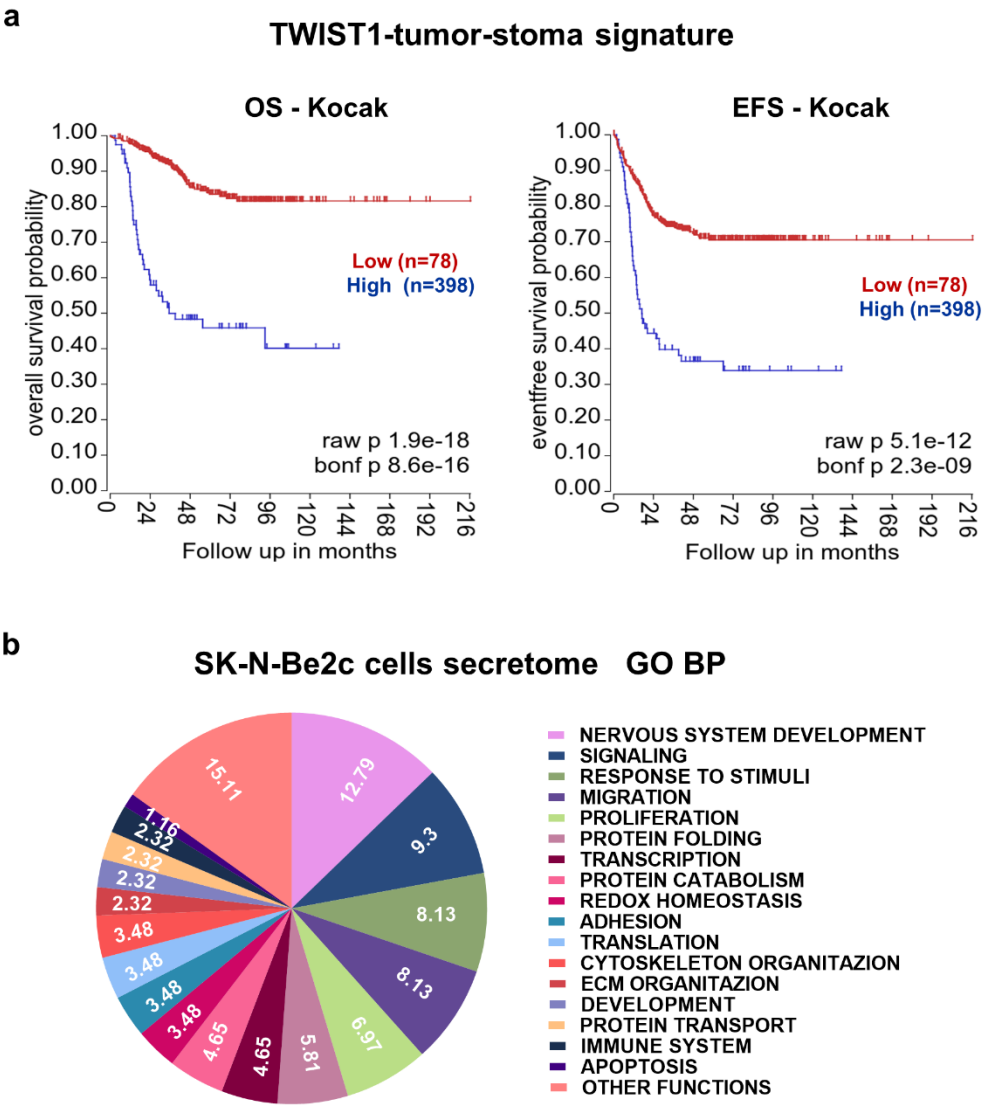

121

122

123 **Supplementary Fig. 9**. **Correlation between the TWIST1-tumor-stroma signature in the**
124 **Kocak NB dataset and the outcome of patients.** (**a**) Kaplan-Meier plots showing the
125 correlation between a high level of the paracrine signature expression and a poor OS and EFS
126 of NB patients in the Kocak dataset. Expression cutoff for both curves: 0.14. (**b**) Illustration of
127 biological processes (BP) found enriched by gene ontology analysis for the DE proteins in SK-
128 N-Be2c cell secretome. Data are reported as the repartition (in %) of the diverse BP identified
129 with a FDR < 0.01 (n=50).

130

131 # Supplementary Figure 10

132

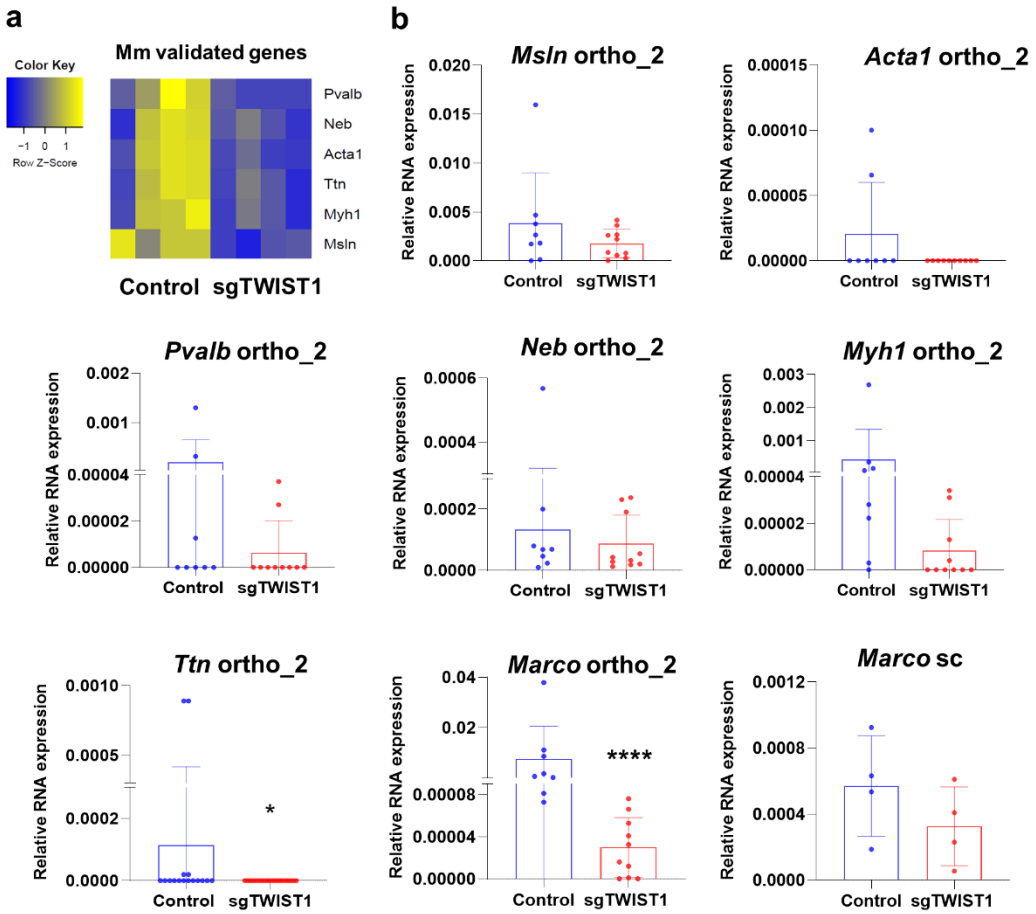

133

134 **Supplementary Fig. 10**. **Validation of selected genes of the myofibroblast signature in**
135 **the ortho_2 and sc tumors by real-time PCR.** (**a**) Heatmap showing the RNA expression
136 levels (z-score) of the Myofibroblasts signature selected genes as determined by RNAseq
137 analysis in ortho_1 tumors. (**b**) mRNA expression levels for the selected myofibroblast genes
138 and *Marco* relative to *β-actin* as determined by RT-qPCR. Data are plotted as individual values
139 with mean ± SD. Mann Whitney test: Ortho_2: *Ttn*: *p= 0.0309; *Marco*: ****p<0.0001. Ortho_2
140 tumors: Control n=8; sgTWIST1 n=10; sc tumors: Control n=4, sgTWIST1 n=4.

141

142